

10

Io's atmosphere

Emmanuel Lellouch, Melissa A. McGrath, and Kandis Lea Jessup

10.1 INTRODUCTION, EARLY STUDIES, AND MAIN ISSUES

Our knowledge of Io's atmosphere has undergone a major revision in the last fifteen years. By 1990, observational information was restricted to several clear but indirect pieces of evidence, a single direct infrared detection by *Voyager* in 1979, and a number of upper limits from ultraviolet spectroscopy. Even loosely constrained, Io's atmosphere was quickly recognized as bearing unique features among planetary atmospheres, the most prominent being its apparent spatial and temporal variability, and possible direct relationship to Ionian volcanism. This lack of data did not hinder, in the 1980–1990 decade, theoretical studies on the horizontal, vertical, and chemical structure of Io's atmosphere. Since 1990, the direct detection of Io's atmosphere from Earth or Earth orbit in different wavelength ranges, along with recent results on Io volcanism and surface composition from *Galileo*, has given a much firmer basis to our perception of Io's atmosphere, justifying, in turn, the development of more elaborate chemical, thermal, dynamical, and volcanic models. In this chapter, we focus on these recent observational and theoretical developments. Earlier studies, which were extensively covered in previous reviews by Johnson and Matson (1989), Trafton *et al.* (1995), Lellouch (1996), and Spencer and Schneider (1996) are only briefly covered here. The reader is also referred to the comprehensive review of McGrath *et al.* (2004) for additional details and figures.

The first definite evidence for an atmosphere around Io was obtained in 1973 with the *Pioneer 10* detection of relatively dense ionospheric layers above Io's surface near the terminator (Kliore *et al.*, 1974, 1975). Very different ionospheric profiles (termed "dayside" and "nightside", although both actually occurred very close to the terminator) were detected at entry and exit and preliminary estimates of the neutral atmosphere required to explain these data yielded surface pressures of 10^{-8} – 10^{-9} bars. Shortly after, optical observations detected atomic sodium around Io (Brown, 1974), and it was quickly established that the observed sodium formed a neutral cloud

of atoms in orbit around Jupiter that had escaped non-thermally from Io, implying a source of Na in Io's atmosphere or at the surface. Further evidence for atmospheric escape was obtained from the optical detection of a potassium cloud (Trafton, 1975) and of ionized sulfur in the magnetosphere (Kupo *et al.*, 1976). In 1979, *Voyager* observations confirmed the importance of sulfur and oxygen ions in Jupiter's magnetosphere (e.g., Broadfoot *et al.*, 1979; Bridge *et al.*, 1979).

The "watershed event" for Io's atmosphere occurred the same year with a triple discovery: the presence of active volcanism on Io's surface (Morabito *et al.*, 1979), the attribution of a 4.1 μm feature in Io's infrared spectrum to solid SO_2 (Fanale *et al.*, 1979; Smythe *et al.*, 1979), and the detection of gaseous SO_2 at 7.3 μm over the volcanic center Loki Patera by *Voyager*/infrared imaging spectrograph (IRIS) (Pearl *et al.*, 1979). The IRIS spectrum was interpreted as indicating a 10^{-7} bar local atmosphere at 130 K (column density = $5 \times 10^{18} \text{ cm}^{-2}$), although a subsequent reinterpretation (Lellouch *et al.*, 1992) has shown it to be consistent with lower pressures (5–40 nanobar, i.e., $(2.5\text{--}20) \times 10^{17} \text{ cm}^{-2}$) and higher temperatures (up to 400 K). Note that Loki was the only region with enough 7 μm continuum radiation to illuminate any SO_2 gas, so that the *Voyager* observation, in itself, did not rule out a global atmosphere. After this single observation, Io's atmosphere eluded further detection for another 11 years, but several attempts in the ultraviolet were useful at placing upper limits on the global SO_2 amount. The most significant result was obtained by Ballester *et al.* (1990) from the International Ultraviolet Explorer (IUE), who placed an upper limit of $2 \times 10^{17} \text{ cm}^{-2}$, for a homogeneous SO_2 atmosphere, implying, by comparison with the *Voyager* result, a strong horizontal non-uniformness.

The early and *Voyager* discoveries represented an enormous step forward, but immediately raised the *essential* question that is still probably focusing most research efforts on Io's atmosphere. Was SO_2 gas detected around Loki because Loki emitted a SO_2 -rich volcanic plume, or rather because the SO_2 frost in that region was able to sustain a significant atmosphere? Indeed, given the SO_2 sublimation vapor pressure curve, a 0.1 μbar atmosphere is in equilibrium with SO_2 frost at 130 K, a reasonable temperature for Io's surface. Extending this issue to Io's atmosphere as a whole, the basic questions were: Is Io's atmosphere primarily supported by sublimation equilibrium, or dynamically maintained by volcanic output? How far does a plume atmosphere propagate horizontally? Is the atmosphere, away from volcanic centers, collisionally thin or thick to the penetration of thermal ions from the plasma torus? Can the atmosphere also be sputter-generated? Did the *Pioneer 10* observations suggest a global atmosphere but with substantial lateral variations?

These limited observations set the stage for the development of models. Models either addressed the atmospheric vertical thermal and compositional structure, with the prime goal of reproducing the *Pioneer 10* ionosphere with surface conditions indicated by *Voyager*, or were concerned with the horizontal distribution of surface pressure and associated dynamics. It was not until the mid-1990s that the two approaches attempted to merge (see below). Models of the first type included notably the extensive work of Kumar (e.g., 1980, 1985) who established the thermal budget of an SO_2 atmosphere and the basics for its photochemistry. As

detailed below, energy sources for Io's atmosphere include solar ultraviolet heating, plasma ion heating (e.g., Johnson, 1989) and Joule heating (ignored in the early models, and accounted for the first time by Strobel *et al.*, 1994). Aeronomical models at that time generally suggested very warm atmospheres (e.g., 500 K at 20 km altitude, 2,000 K at 80 km). However, these models mistreated or ignored non-local thermodynamic equilibrium (LTE) SO₂ infrared cooling, and omitted rotational cooling. Photochemical models of a pure SO₂ or of an SO₂-Na atmosphere, including ionospheric chemistry, were developed (e.g., Kumar, 1985; Summers, 1985). Though these models had only moderate success in reproducing the *Pioneer 10* ionospheric density profiles, they did indicate that Io's atmosphere must also contain significant amounts of SO, O₂, and atomic S and O. Given the estimated supply rates to the torus, about 1×10^{28} and $4 \times 10^{27} \text{ s}^{-1}$ for O and S respectively, it was realized that Io's atmosphere has a short lifetime – of the order of 10 days – and must be replenished continuously to offset its escape loss.

Early models describing the horizontal distribution of the SO₂ atmosphere fell into three categories: “buffered”, “dynamical”, and “sputtered”. In buffered models, the distribution of gas reflects strict local vapor pressure equilibrium with the surface ice. Most of the models assumed uniform frost coverage, but varied in the estimate of the frost temperature controlling the atmospheric pressure. Variants included the “equilibrium model”, the “regional cold-trapping model” (both described by Fanale *et al.*, 1982), and the “subsurface cold-trapping model” of Matson and Nash (1983). Due to the very steep SO₂ vapor pressure curve with temperature, the associated pressures differed by orders of magnitude, and the models predicted enormous pressure variations with solar zenith angle (SZA). Dynamical models (Ingersoll *et al.*, 1985; Ingersoll, 1989; Moreno *et al.*, 1991) addressed the issue of pressure redistribution from supersonic winds, creating regions of net sublimation in an equatorial band and regions of net condensation at mid-latitudes (30°–70°). These models were extended to the case of non-uniform frost and of volcanic atmospheres. Ingersoll (1989) developed the concept of “averaging length” (i.e., the characteristic dimension (of order 50–100 km) over which each frost patch controls its own pressure), and established the equivalence between volcanic venting and sublimation in maintaining the surface pressure. For both sources, the key factor controlling the areal extent of the atmosphere remains the frost temperature distribution, so these studies left open the possibilities of patchy and extended atmospheres on Io. Because sublimating SO₂ frosts are losing mass, the ultimate source of Io's atmosphere is volcanic output. Nonetheless, the distinction between buffered and volcanic atmospheres is significant as the associated vertical structures (hydrostatic and plume-like, respectively) are very different, with dynamical, thermal, and compositional implications. In addition, a sublimation atmosphere probably collapses at night and in eclipse, while a volcanic atmosphere does not. Sputtering models (see review in Cheng and Johnson, 1989) demonstrated that the impact of energetic magnetospheric particles onto the surface can generate a giant rarefied atmosphere. Such an atmosphere, or “corona”, is self-limited to $\sim 10^{16} \text{ cm}^{-2}$ since sufficient gas build-up halts further ion penetration, but the mechanism may still be the dominant source of atmosphere in some specific locations (e.g., high-latitude, nightside). The case of

sputtering of a pre-existing, collisionally thick atmosphere was also studied (McGrath and Johnson, 1987).

10.2 RECENT OBSERVATIONAL PROGRESS

10.2.1 The SO₂ atmosphere

Millimeter observations

Since the first detection of SO₂ gas in emission in a rotational line at 222 GHz in January 1990 (Lellouch *et al.*, 1990), millimeter-wave heterodyne spectroscopy has provided a new technique to probe Io's atmosphere. Such observations were acquired mostly with the IRAM 30-m telescope, and yielded useful data in 1991, 1993, 1994, 1995, 1999, and 2002. These observations do not resolve Io's disk, are concentrated around maximum eastern elongation (orbital longitude $L = 90^\circ$) or western elongation ($L = 270^\circ$), and have low temporal (i.e., longitudinal) resolution. They thus primarily sample the dayside leading and trailing sides (as opposed to the sub-Jovian and anti-Jovian hemispheres).

A dozen SO₂ lines have been detected over the years. They span a factor of ~ 20 in line intensity, but with one exception all have relatively low energy levels ($8\text{--}165\text{ cm}^{-1}$). They result from LTE thermal emission of the atmosphere (Lellouch *et al.*, 1992). All detected SO₂ lines appear in emission (Figure 10.1). Line contrasts reach 20–40 K in brightness temperature, implying that the mean dayside SO₂ gas temperature is higher than the mean surface brightness temperature, by at least 20–40 K, and maybe by much more, if the dayside atmosphere covers only a fraction of Io's surface and/or if the lines are not optically thick.

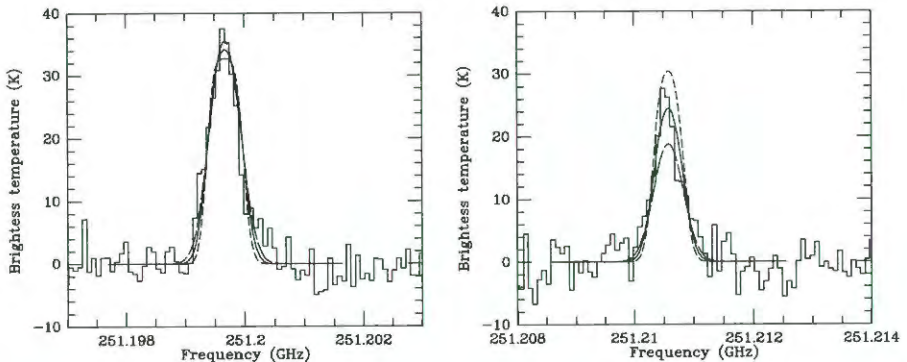


Figure 10.1. Illustration of temperature determination from SO₂ millimeter observations. The 251.2 GHz SO₂ doublet, observed on 26 November 1999 on Io's trailing side, is here compared with three hydrostatic models. Solid line: atmospheric temperature $T_{\text{atm}} = 400\text{ K}$, surface pressure $p = 2.7\text{ nbar}$ (i.e., $1.4 \times 10^{17}\text{ cm}^{-2}$), projected atmospheric coverage $f_p = 14\%$. Short-dashed line: $T_{\text{atm}} = 250\text{ K}$, $p = 1.7\text{ nbar}$, $f_p = 20\%$. Long-dashed line: $T_{\text{atm}} = 600\text{ K}$, $p = 2.5\text{ nbar}$, $f_p = 26\%$. For each temperature, the surface pressure is determined by fitting the line width. The relative line contrast is best fit for $T_{\text{atm}} = 400\text{ K}$ (from Lellouch *et al.*, 2000).

The observed lines, fully resolved, are generally symmetric about their central frequency, although the most recent observations may suggest more complex line-shapes. The line width of the strongest lines (full width at half-maximum, FWHM) is ~ 600 kHz at 220 GHz and scales as the line frequency, indicating Doppler broadening – collisional broadening would anyway imply an implausible 10^{-4} bar surface pressure. The line FWHM/frequency ratio, $\sim 2.7 \times 10^{-6}$, gives a temperature of 910 K for thermal broadening, or a velocity of 0.8 km s^{-1} for bulk velocity broadening.

The first interpretation of these data (Lellouch *et al.*, 1990, 1992) assumed Io's SO_2 atmosphere to be in hydrostatic equilibrium. In this case, $T_{\text{atm}} = 910 \text{ K}$ is an upper limit to the mean atmospheric temperature. Since the bulk of Io's atmosphere is likely to be at a much colder temperature (see radiative models below), the line widths were interpreted as being affected by saturation effects. In this framework, the analysis of a single strong line indicates that the atmosphere is comfortably collisionally thick (5×10^{16} to $5 \times 10^{17} \text{ cm}^{-2}$ column density) but covers a restricted fraction of Io's disk. A more precise characterization, however, requires multi-line observations, whereby the relative contrast of several lines of different strengths constrain their saturation degree and helps disentangle the opacity/temperature/column density/coverage variables. The “atmospheric coverage” observable is f_p , the fraction of the projected surface (disk) covered by the atmosphere. Converting f_p to actual *hemispheric coverage* f_h , requires knowing how the gas is distributed. A common assumption is that the atmosphere is restricted to a circular region around disk center (i.e., close to the subsolar point, in which case $f_h = 1 - (1 - f_p)^{1/2}$).

The need for “multi-line” observations motivated most of the SO_2 millimeter-wave observations over 1991–1999. In retrospect, they did not give a completely consistent picture of Io's atmosphere, especially regarding the mean atmospheric temperature and the fractional coverage of the atmosphere. The early observations (1991–1994) indicated a very hot ($T_{\text{atm}} = 500\text{--}600 \text{ K}$), dense (surface pressure $\sim 3\text{--}15 \text{ nbar}$), and very localized ($f_p = 5\text{--}8\%$, $f_h = 2.5\text{--}4\%$) atmosphere on the trailing side, and a somewhat cooler ($250\text{--}400 \text{ K}$) and more extended ($f_p = 12\text{--}16\%$, $f_h = 6\text{--}9\%$) atmosphere on the leading (Lellouch *et al.*, 1992; Lellouch, 1996). In all these observations, the hemispheric-average column density was in the range $(1\text{--}2) \times 10^{16} \text{ cm}^{-2}$, with a tendency for higher values on the trailing than on the leading. Subsequent observations (1999) confirmed this general picture, but provided somewhat different temperature and atmospheric coverage numbers, namely $T_{\text{atm}} = 400 \text{ K}$ and $f_h = 8\%$ on the trailing side vs. $T_{\text{atm}} = 200 \text{ K}$ and $f_h = 24\%$ on the leading (Lellouch *et al.*, 2000). In contrast, the January 2002 observations (leading + trailing), which included a high-energy (404 cm^{-1}) line, indicated a rotational temperature of only $180 \pm 60 \text{ K}$ (Lellouch *et al.*, 2003). Thus, the gas temperature estimated from these multi-line observations has decreased over the years, and it is unclear if this is due to actual variability or to signal-to-noise limitations in the early data sets.

Although the SO_2 millimeter emissions are permanently detectable, temporal and orbital variability can be directly seen on the data themselves. A clear example was observed in June 1995, with an unusually sharp 143-GHz line compared with other years (Lellouch, 1996). The most likely interpretation is an increase of the atmospheric

areal extent, along with a decrease of either the surface pressure or gas temperature. In fact, this observation, unlike all other millimeter observations, is consistent with a global atmosphere. Strong lines observed in 1999 were about 50% stronger than in 1990–1994 (McGrath *et al.*, 2004, Figure 1), interpreted as a generally higher surface coverage. The unprecedented S/N levels of the 1999 observations allowed the exploration of orbital variations of line characteristics beyond the leading/trailing contrast. The main findings are: (i) a suggested increase in the integrated line strengths over $L = 40\text{--}135$ and a decrease over $L = 240\text{--}340$; (ii) a more definite variation of line frequency with orbital position, with a global blueshift by $\sim 100\text{ m s}^{-1}$ on the leading side and a similar redshift on the trailing side. The interpretation remains uncertain, although it might be related either to volcanic plume emission geometry (see below) or to angular momentum transfer from the plasma flow hitting Io's trailing side at $\sim 57\text{ km s}^{-1}$ (see discussion in McGrath *et al.*, 2004).

The high temperatures on at least the trailing side inferred from the early millimeter observations are at odds with radiative–conductive models (Strobel *et al.*, 1994) which predict that the atmosphere never warms above 200 K in the first scale height. This may suggest that the hydrostatic interpretation of the millimeter data is incorrect. Ballester *et al.* (1994) first proposed that the millimeter line widths primarily reflect velocity dispersion within gaseous plumes rather than a combination of temperature and saturation effects. Lellouch (1996) presented simplified models based on this idea. The introduction of a new parameter, namely the plume ejection velocity, controlling the line widths, relaxes the constraints on the gas temperature. The hemispheric-average column densities of $(0.6\text{--}2.5)\times 10^{16}\text{ cm}^{-2}$ obtained in these models are comparable with those in the hydrostatic models, but the data can now be fit even with low temperatures, and therefore the atmosphere is no longer necessarily “hot and localized” – a typical surface coverage is then $f_h \sim 30\%$ for an assumed $T_{\text{atm}} = 200\text{ K}$. However, because the plumes are small (e.g., $r = 135\text{ km}$ for an ejection velocity of $\sim 0.5\text{ km s}^{-1}$ as indicated by the data), they must be very numerous (50–300) to cover a significant fraction of one hemisphere. This large number may be somewhat decreased if allowance is made for a non-zero horizontal flow which increases the plume size. This number can be reduced further if a mixture of small and Pele-class plumes is assumed. With the ~ 150 active volcanic centers observed by *Galileo* (Lopes-Gautier *et al.*, 1999; Lopes *et al.*, 2004), 50 active plumes may not be unreasonable, especially if many of them are the invisible “stealth” plumes (i.e., those with a low condensate content) postulated by Johnson *et al.* (1995). The possible existence of almost purely gaseous plumes has been demonstrated by Kieffer (1982) in the case of a high-entropy erupting fluid from a reservoir of superheated SO_2 vapor in contact with a deep, hot, and dense silicate melt (1,400 K, 40 bar). While already complex to implement, the plume models presented by Lellouch (1996) certainly represent a rough and simplistic description of the complex physics of volcanic plumes (see Section 3.3, and Chapter 8).

Ultraviolet observations

SO_2 gas absorbs strongly in the ultraviolet region. Since 1992, this has been exploited in numerous successful ultraviolet observations, starting with the first ultraviolet

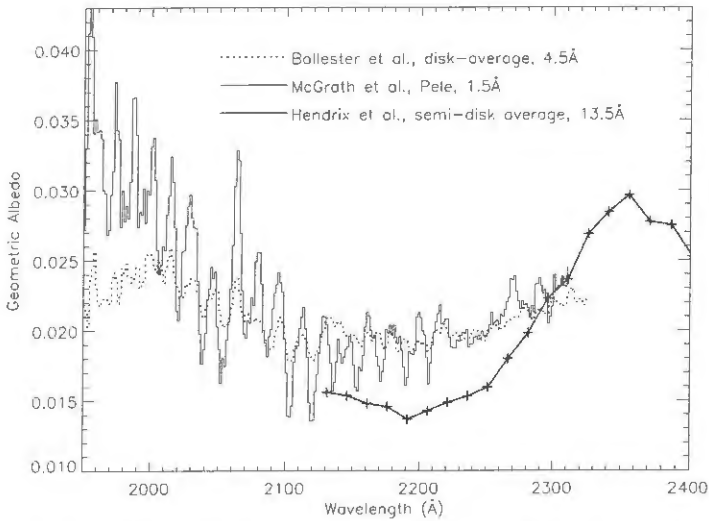


Figure 10.2. Comparison of three mid-ultraviolet spectra of Io, illustrating the importance of spectral resolution in detecting SO_2 in Io's atmosphere (from McGrath *et al.*, 2004). For each observation, the spectral resolution, in Angstroms, is indicated.

images of Io (Paresce *et al.*, 1992) and the first spectroscopic detection of SO_2 in the ultraviolet (Ballester *et al.*, 1994). Spectroscopic observations divide between disk-averaged (Ballester *et al.*, 1994; Trafton *et al.*, 1996; Jessup *et al.*, 2005) and disk-resolved (Hendrix *et al.*, 1999; McGrath *et al.*, 2000; Spencer *et al.*, 2000; Jessup *et al.*, 2004a) measurements. Unlike the millimeter-wave spectrum, the ultraviolet spectrum is primarily sensitive to the column-integrated abundance of the absorbing gases, but not directly for their temperature, except for a general decrease in the band contrast with increasing temperature and subtle variations in the band peak position and skewness (see e.g., Wu *et al.*, 2000). Analysis is subject to two complications. The first one comes from the fact that, as pointed out by Belton (1982), the SO_2 ultraviolet spectrum has a very complex structure of many densely packed lines that has not been resolved in laboratory measurements, so that line-by-line position and intensity information is not available. In this situation, applying Beer's law at a spectral resolution comparable with that of the measurements can lead to significant underestimates of absorber abundance. Band models are much preferred, and several modelers have followed the treatment by Ballester *et al.* (1994). The other complication is due to the poorly known contribution of Io's surface to the overall geometric albedo. Indeed, SO_2 frost, present on Io's surface, has broadly similar spectral properties as SO_2 gas; while SO_2 frost is known to be dark in the ultraviolet, it is impossible to reliably predict the absolute surface reflectance and its spectral dependence. As a consequence, only observations with a spectral resolution enabling us to distinguish characteristic gas spectral features unambiguously constrain gas abundances (Figure 10.2).

This situation has led, in particular, to competing interpretations for the imaging data. For example, the early ultraviolet images of Sartoretti *et al.* (1994, 1996) can be

modeled either purely in terms of variations of surface properties, or by assuming that the darkest regions seen in the images represent SO₂ gas. The latter explanation was preferred by Sartoretti *et al.* (1996), who concluded to the presence of SO₂ patches (one of which is Pele) with typical column densities of $\sim 1 \times 10^{18} \text{ cm}^{-2}$, covering 11–15% of the projected surface. Because these early ultraviolet images were insensitive to SO₂ column densities below $\sim 8 \times 10^{16} \text{ cm}^{-2}$, the presence of a lower density component could not be ascertained.

Disk-averaged spectroscopic observations were initially obtained in 1992 with the Hubble Space Telescope (HST) Faint Object Spectrograph (FOS) and Goddard High-Resolution Spectrograph (GHRS) instruments (Ballester *et al.*, 1994; Trafton *et al.*, 1996), covering altogether the 1,975–2,350 Å range. Additional data with HST/FOS were acquired in 1994 and 1996 (Jessup *et al.*, 2005). Not surprisingly in view of the lack of spatial resolution, the data can generally be fit by a variety of models, ranging from hemispherically uniform to localized (either in latitude bands or in spatially confined patches) atmospheres. Typically, uniform models indicated SO₂ column densities of $(5\text{--}10) \times 10^{15} \text{ cm}^{-2}$. Patchy atmospheres were found to satisfy the data, provided that the local column densities remained below $(1\text{--}3) \times 10^{17} \text{ cm}^{-2}$ and the hemispheric coverage (f_h) exceeded 8–23% (Ballester *et al.*, 1994; Trafton *et al.*, 1996). Cold temperatures ($T_{\text{atm}} = 110\text{--}250 \text{ K}$) are preferred. Jessup *et al.* (2005) found that a two-component model, consisting of a low-density ($10^{15}\text{--}10^{16} \text{ cm}^{-2}$) component covering 50–100% of the observed hemisphere and a high-density ($10^{17}\text{--}10^{18} \text{ cm}^{-2}$) component, restricted to 2–10% of the surface, provided an optimum match to the 1994–1996 FOS data. The 1994 and 1996 FOS data show somewhat deeper absorptions on the leading side than on the trailing side. From optimized fits, Jessup *et al.* (2005) interpret these variations as being due to a larger SO₂ column density on the leading side in 1996 ($(3\text{--}4) \times 10^{16} \text{ cm}^{-2}$ vs. $(1\text{--}3) \times 10^{16} \text{ cm}^{-2}$ on the trailing for an atmosphere covering a $\pm 30^\circ$ equatorial band), and a possibly higher gas temperature on the trailing side in 1994. The first of these conclusions is moderately inconsistent with the finding by Trafton *et al.* (1996) of a 30% denser atmosphere on the trailing side than on the leading in 1992. Nonetheless, a global analysis of the FOS and GHRS data, assuming an atmosphere distributed uniformly across the disk, indicates that the disk-average column densities did not vary temporally by more than a factor of 2 between 1992 and 1996.

Another important feature of the ultraviolet spectrum of Io, first noted from HST/FOS data at 2,250–3,300 Å, is the absence of fine structure due to SO₂ bands in the near-ultraviolet ($\lambda > 2,500 \text{ Å}$). Clarke *et al.* (1994) interpreted this as ruling out a global atmosphere denser than $4 \times 10^{16} \text{ cm}^{-2}$. However, they indicated that a very dense, localized component (e.g., $2 \times 10^{19} \text{ cm}^{-2}$ over a 10% area), was not inconsistent with the data. At such very high column densities, the 2,800–3,100 Å range is saturated to 100% absorption, even in the continuum between lines, consequently showing no spectral contrast. Hendrix *et al.* (1999), using the *Galileo* ultraviolet spectrometer, obtained a spectrum of similar spectral resolution and coverage (though extending down to 2,100 Å) as that of Clarke *et al.* (1994). Though their spectrum did not resolve the individual SO₂ multiplets (Figure 10.2) and was limited to a single large aperture, covering the 120°W–150°W longitudes and encompassing all latitudes, these data

provided the first disk-resolved observations of Io's atmosphere. In addition to the features described by Clarke *et al.* (1994), a clear decrease of the albedo shortward of 2,360 Å was observed. Hendrix *et al.* (1999) attributed this behavior to SO₂ gas absorption, and inferred very large ($1 \times 10^{19} \text{ cm}^{-2}$) column densities over 25% of the aperture. They also found that 35% of the observed surface is covered by a $4 \times 10^{17} \text{ cm}^{-2}$ component, the remaining 40% being gas-free.

In spite of their inherent ambiguity, these various observations lent credit to the idea of spatial variations in Io's surface pressure. These variations were finally demonstrated by the spatially resolved HST/FOS 1996 observations of McGrath *et al.* (2000). The targets were chosen to sample different physical conditions that are likely to exist on Io's surface: (1) the Pele Volcano (18°S, 257°W); (2) Ra (7°S, 318°W), a potentially active region bright in the visible and dark in the ultraviolet, indicating abundant SO₂ frost; and (3) a reference region at 45°S and 300°W, designated as "T3", dark in visible and bright in ultraviolet (i.e., presumably frost-poor). All three targets were within 10° of the subsolar longitude at the time of observation. The spectral resolution (1.5 Å), spatial resolution (0.26''), and S/N were unprecedented in these observations (Figure 10.2). Best fit SO₂ column densities and temperatures were found to be $3.25 \times 10^{16} \text{ cm}^{-2}$, $1.5 \times 10^{16} \text{ cm}^{-2}$, and $7 \times 10^{15} \text{ cm}^{-2}$, and 280, 150, 200 K, for Pele, Ra, and T3 respectively. The interpretation of the differences in SO₂ column density, however, remains uncertain because the degree of volcanic activity, especially at Ra, during the observations was unknown. It is, in particular, hard to know whether the difference between Pele and Ra is due to a difference in activity, or to a longitudinal variation of the low-latitude sublimated SO₂ column density (Spencer *et al.*, 2005). In any case, the observation of SO₂ at T3 – a region in which no active plume has ever been observed – was strong evidence for a relatively widespread atmosphere, and the factor-of-two (only) lower column density measured at T3 compared with Ra indicated a drop in SO₂ pressure with latitude being much more gradual than predicted by the early sublimation models (McGrath *et al.*, 2000).

From imaging of the Pele plume against dark sky and silhouetted against Jupiter during Io transit, performed only 7 days after the McGrath *et al.* (2000) observations, Spencer *et al.* (1997) determined its height and 2,720 Å opacity. The plume was not detected at 3,400 and 4,100 Å. This wavelength-dependent optical depth was interpreted as due to absorption by either small dust particles or SO₂ gas with $3.7 \times 10^{17} \text{ cm}^{-2}$ column density. However, as discussed below, HST/STIS (Space Telescope Imaging Spectrograph) observations of the Pele plume in 1999 indicated much lower (factor-of-10) SO₂ column densities in the plume (Spencer *et al.*, 2000) and a series of strong absorption lines due to gaseous S₂ at 2,400–3,100 Å. In retrospect, this indicates that the source of opacity in the Pele images was primarily absorption by S₂, with negligible dust extinction and only a minor contribution due to gas SO₂. This also probably applies to the 2,600 and 2,850 Å images presented by Sartoretti *et al.* (1994, 1996).

Building upon the results of McGrath *et al.* (2000), a more complete investigation of the longitudinal and latitudinal distribution of Io's SO₂ atmosphere was achieved by Jessup *et al.* (2004a). They used HST/STIS with a 0.1''-wide slit, centered over the Prometheus plume and oriented at ~45°, to sample regions, with and without

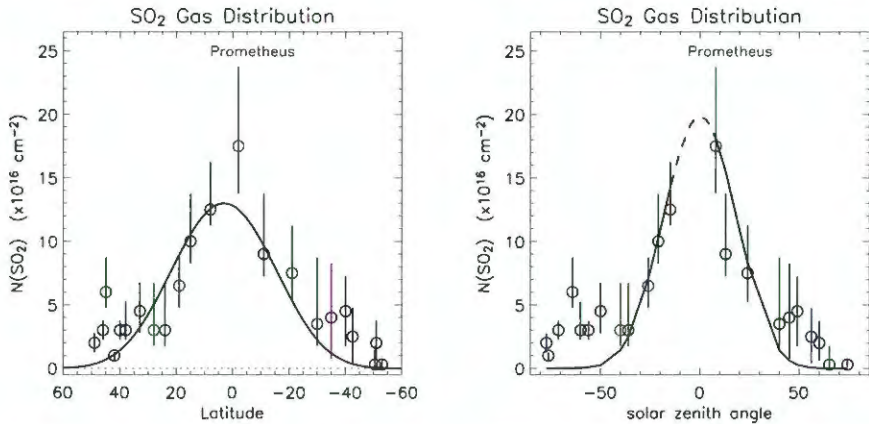


Figure 10.3. SO_2 gas distribution as a function of latitude and solar zenith angle, determined from HST/STIS observations (Jessup *et al.*, 2004). Results are compared with predictions from two versions of a simple sublimation model (see text for details).

active volcanic hot spots, on the anti-Jovian hemisphere, extending $\pm 50^\circ$ latitude. The inferred SO_2 column densities peaked at $1.25 \times 10^{17} \text{ cm}^{-2}$ near the equator (i.e., eight times the value determined by McGrath *et al.*, 2000, for Ra), with an additional $5 \times 10^{16} \text{ cm}^{-2}$ enhancement over Prometheus, which corresponds to a volcanic output of $\sim 10^4 \text{ kg s}^{-1}$ (and not 10^5 kg s^{-1} as stated in Jessup *et al.*). Although the slit encompassed several volcanic hot spots or plume sites (e.g., Volund, Zamama, Tupan, Malik), no local SO_2 enhancement was detected besides the one at Prometheus. The SO_2 column densities fall off smoothly as a function of latitude or SZA (Figure 10.3). Although the slit orientation and the absence of diurnal monitoring in this single observation prevented disentangling longitudinal (i.e., geographical), diurnal, and latitudinal variations, it appears that below $\pm 30^\circ$ latitude, the data can well be matched by a simple sublimation model with a subsolar/equatorial frost temperature of $117.3 \pm 0.6 \text{ K}$ and frost temperatures either: (i) in instantaneous equilibrium (SZA control); or (ii) in equilibrium with diurnally averaged sunlight (latitudinal control). In contrast, the decrease in SO_2 away from Prometheus is slower than expected from a single isolated volcanic source (Zhang *et al.*, 2003). At mid-latitudes ($30\text{--}50^\circ$), the decrease in the SO_2 column density with latitude is much shallower than predicted by the two versions of the simple sublimation model, confirming the McGrath *et al.* (2000) result based on the comparison between Ra and T3. This behavior could result from a latitudinal decrease of the frost albedo, an increase of pressure due to hydrodynamic flow (as discussed hereafter in Section 10.3.5), or the presence of active volcanic venting at these latitudes. Nonetheless, the Jessup *et al.* (2004a) results were generally interpreted as supportive of the sublimation atmosphere concept, and, when compared with the McGrath *et al.* (2000) results, provided the first clear evidence for dramatic longitudinal variations. Finally, these observations revealed the first detection of near ultraviolet ($2,800 \text{ \AA}$) continuum emission, which appears to be correlated with the inferred SO_2 columns.

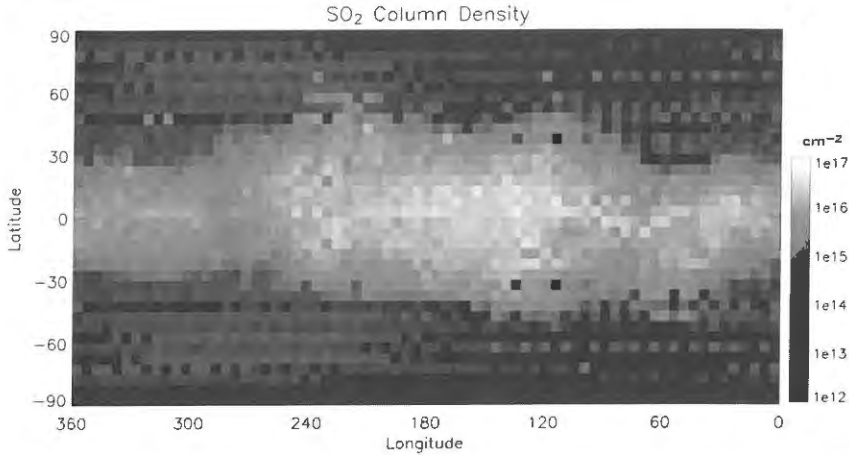


Figure 10.4. 2-D SO₂ gas distribution, as inferred from Ly α images (from Feaga *et al.*, 2004a). (See also color section.)

The most global view of Io's SO₂ atmosphere at spatial scales >200 km is provided by the analysis of HI Ly α images acquired by HST/STIS over 1997–2001. These images, first obtained by Roesler *et al.* (1999), show that the Ly α reflectance pattern consists of two mid-to-high latitude ($>45^\circ$) bright patches at the 2 kR level, while the equatorial latitudes are dark, with ~ 0.7 kR at disk center. Though Roesler *et al.* (1999) envisaged several explanations for the observed structure, the explanation of absorption of surface-reflected solar Ly α by low-latitude atmospheric SO₂ was shown to be the most likely by Feldman *et al.* (2000) and Strobel and Wolven (2001), as SO₂ is a strong continuum absorber at Ly α (cross section $\sigma = 3.9 \times 10^{-17}$ cm²). This interpretation is consistent with the absence of bright polar regions during eclipse (McGrath *et al.*, 2004). Using various assumptions on the surface reflectivity at Ly α , Feldman *et al.* (2000) found equatorial SO₂ column densities in the range $(0.5\text{--}4) \times 10^{16}$ cm⁻². Strobel and Wolven (2001) analyzed one of these images by constructing spatial models of the Ly α emission, based on longitudinally homogeneous model atmospheres with column densities decreasing sharply from $(1\text{--}1.7) \times 10^{16}$ cm⁻² to $\sim 3 \times 10^{14}$ cm⁻² poleward of 50° latitude. These models capture the essential observational features and suggest that Io's atmosphere is restricted to a $\pm 30\text{--}40^\circ$ band in which lateral inhomogeneities (at the resolution of the data) are modest. Strobel and Wolven (2001) interpreted this in the context of numerous (10–200) plume atmospheres, with a total emission rate of $\sim 5 \times 10^{30}$ s⁻¹. A more comprehensive study of the Ly α images was performed by Feaga *et al.* (2004). They found that the data show a fairly stable latitude/longitude pattern (Figure 10.4), in which the region of strong Ly α attenuation extends to higher latitudes ($\sim \pm 40^\circ$) on the anti-Jovian hemisphere than on the sub-Jovian side ($\sim \pm 25^\circ$). Modeling of these data indicated maximum column densities $\sim 1 \times 10^{16}$ cm⁻² on the sub-Jovian hemisphere and ~ 4 times higher on the anti-Jovian. There is overall little, if any, evidence for temporal – as opposed to

longitudinal – variability in the Ly α data, though the low SO₂ column density at 45°S ($\sim 3 \times 10^{14}$ (i.e., a factor of 25 smaller than the McGrath *et al.* (2000) measurement at T3) may indicate time variations. Note finally that the Ly α images show limb-to-limb atmospheric absorption, and therefore no evidence for a diurnal variation of the SO₂ column densities.

Infrared observations

Ground-based, disk-averaged, mid-infrared observations of Io, performed over 2001–2005 at NASA/IRTF (Infrared Telescope Facility), led to the detection of ~ 15 lines belonging to the ν_2 band of SO₂ at 519–531 cm⁻¹, achieving the first infrared detection of SO₂ in Io's atmosphere since the *Voyager* discovery (Spencer *et al.*, 2005). With possible marginal exceptions, lines were always observed in absorption. Dramatic variations in line depth as a function of orbital longitude were observed, with the strongest feature at 530.412 cm⁻¹ varying from 7% absorption at L = 180 to 1% at L = 315, at an observed resolution of 57,000. Unlike in the millimeter observations, thermal emission in the mid-infrared occurs in a strongly non-LTE regime, with important radiative exchanges with the surface and deep space. This complicates the analysis considerably, since the associated source function, as characterized by the vibrational temperature as a function of altitude, depends on the combination of atmospheric kinetic temperature (unknown but assumed to be horizontally and vertically constant), atmospheric density, and surface temperature distribution. As a consequence, the line depths do not uniquely determine the atmospheric conditions. Nonetheless, the maximum line depths indicate that the mean gas temperature is surprisingly low (below ~ 150 K), and the most plausible interpretation of the data is that the equatorial column density varies from $\sim 1.5 \times 10^{17}$ cm⁻² at L = 180 to $\sim 1.5 \times 10^{16}$ cm⁻² near L = 300, generally consistent with ultraviolet spectroscopy and imaging. Comparison of data taken in 2001, 2002, 2004, and 2005 indicate that, with the possible exception of longitudes near 180 between 2001 and 2002, the SO₂ column densities are very stable with time, and in particular did not decrease between 2001 and 2005. Since this period corresponded to a recession of Io from the Sun, presumably accompanied by a cooling of its surface frosts, the constancy of the SO₂ columns possibly argues for a dominantly volcanic support of the atmosphere.

10.2.2 Minor molecular species

Beyond SO₂, a number of other molecular compounds have been successfully searched for in Io's atmosphere. A special effort was made on SO, which was predicted to be a significant species by all photochemical and thermo-chemical models (e.g., Kumar, 1982, 1985; Wong and Johnson, 1996; Summers and Strobel, 1996; Zolotov and Fegley, 1998a). The first detection of SO was achieved from millimeter observations (Lellouch *et al.*, 1996), and four separate SO lines have now been detected, with a contrast typically half that of the strong SO₂ lines. In the framework of hydrostatic models, the observations cannot distinguish between a

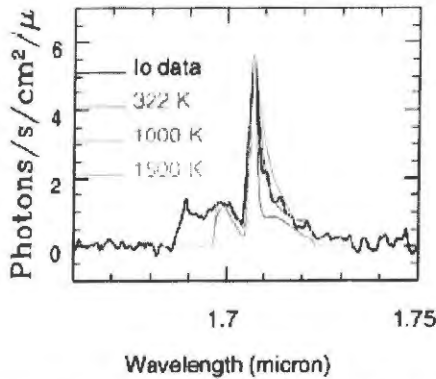


Figure 10.5. The detection of infrared emission from SO in eclipse. The band structure indicates a rotational temperature of $\sim 1,000$ K (from De Pater *et al.*, 2002). (See also color section.)

hemispheric SO atmosphere – in this situation, a barely collisionally thick SO atmosphere with a $(2\text{--}6)\times 10^{14}$ cm^{-2} column density is indicated – and an SO component co-located with SO_2 on a restricted fraction of Io's surface with a 4–10% SO/ SO_2 mixing ratio. In the case of volcanic models, the SO/ SO_2 mixing ratio within the erupting plumes is also in the range 3–10%.

In the ultraviolet, the disk-resolved observations of McGrath *et al.* (2000) are consistent with the presence of SO at a relative mixing ratio of about 10% of SO_2 , consistent with the millimeter-wave detection (and with possible spatial variations), although the unambiguous identification of SO bands in the ultraviolet albedo is very difficult because the SO cross sections are very similar to SO_2 .

A third observation of SO was achieved from infrared spectroscopy of Io during eclipse with Keck II, leading to the detection of the forbidden electronic $a^1\Delta \rightarrow X^3\Sigma^-$ transition of SO at 1.71 μm (De Pater *et al.* 2002, their fig. 5). The detection was later confirmed by Goguen and Blaney (2001). These emissions are thought to originate from volcanic vents, Loki and Janus/Kanehekili for the two observations, respectively. The Keck II observations indicate an emission rate of $\sim 2\times 10^{27}$ photons per second. De Pater *et al.* (2002) discussed many possible mechanisms for this emission and concluded that it was caused by direct ejection of SO molecules in the excited $a^1\Delta$ state from the vent at a $\sim 1,500$ K quenching temperature. Other processes such as solar or electron excitation of SO, electron impact dissociation of SO_2 , or ionospheric recombination of SO_2^+ , all of which can produce excited SO, seem to fail by at least 1–2 orders of magnitude. The shape of the band indicates a $\sim 1,000$ K rotational temperature. Because rotational levels are easily thermalized, this temperature may represent the actual kinetic temperature of the emitting gas as it is vented.

From imaging and spectroscopy of the Pele plume on Io's limb and against Jupiter, Spencer *et al.* (2000) discovered molecular S_2 through 15–20 bands belonging to the $B^3\Sigma_u^- - X^3\Sigma_g^-$ system at $2,500\text{--}3,000$ \AA , in addition to a detection of SO_2 gas at shorter wavelengths. Their tangential SO_2 column density of $\sim 7\times 10^{16}$ cm^{-2} , when converted to a vertical column (\sim factor of 2 decrease) is in remarkably good agreement with the $\sim 3.25\times 10^{16}$ cm^{-2} column density found by

McGrath *et al.* (2000). The S_2 to SO_2 mixing ratio in the plume is 0.08–0.3. This spectacular discovery, though not unexpected (since sulfur vapor has been proposed for a long time to be the driver of the Pele plume (McEwen and Soderblom, 1983)), appears extremely valuable to infer chemical conditions in the volcanic source region. Comparing with the thermo-chemical equilibrium calculations of Zolotov and Fegley (1999), the observed S_2/SO_2 ratio implies equilibration with silicate magmas near the quartz–magnetite–fayalite buffer for a 1,400 K temperature or near the wurstite–magnetite buffer at 1,800 K. The S_2 detection may be the key in explaining the red deposits near Pele and other active regions, as S_2 is unstable against photolysis, producing reddish S_3 and S_4 molecules by polymerization. Additional observations of plume transits on the Io limb in 2003–2004 (Jessup *et al.*, 2004b) indicated a temporal variability of the S_2 abundance in the Pele plume, including periods where the gas was only marginally detected, a positive detection of S_2 near Io's equator, and its prominent absence in Prometheus, in agreement with the McEwen and Soderblom (1983) classification.

The most recently detected molecular species in Io's atmosphere is gaseous NaCl, achieved in January 2002 (Lellouch *et al.*, 2003) from rotational line emission, via the detection of emission lines at 234.252 and 143.237 GHz. The disk-averaged column density is in the range $(0.8\text{--}20) \times 10^{13} \text{ cm}^{-2}$, with a preferred value of $4 \times 10^{13} \text{ cm}^{-2}$ (i.e., about 0.4% of SO_2). Because of its vanishingly low vapor pressure at Io's temperature, the most likely source of NaCl is direct volcanic output, though sputtering of salt-bearing atmospheric aerosols is not excluded. Volcanic plume models indicate total volcanic emission rates of $(2\text{--}8) \times 10^{28}$ NaCl molecules per second (i.e., typically 0.3–1.3% of the SO_2 rates). Though the observational data cannot directly prove it, NaCl is probably restricted to less extended regions than SO_2 because of increased photolytic and condensation losses. The detection of NaCl is important because it provides a source for the sodium clouds surrounding Io (see below).

Eight other compounds (CO , H_2S , OCS , S_2O , ClO , CS , $NaOH$, KCl) were searched for unsuccessfully at millimeter wavelengths. The most significant of the associated upper limits is probably a stringent 10^{-10} bar upper limit on a global H_2S atmosphere (Lellouch *et al.*, 1992). An upper limit of $2 \times 10^{14} \text{ cm}^{-2}$ for the abundance of CS_2 was set by McGrath *et al.* (2000) from ultraviolet observations.

10.2.3 Atomic species

Five atomic species have been identified in Io's atmosphere or more extended neutral clouds. Observations of the strong resonance transitions of Na (and to a lesser extent of K) provide the basis of most of our knowledge of Io's neutral cloud dynamics and interaction with the plasma torus. Since these observations principally probe escaped sodium rather than the bound atmosphere near the surface, they do not, however, provide direct information on the sources of alkalis, the most likely of which are: (i) plasma sputtering of the surface where sodium may occur in different forms (see discussion in McGrath *et al.*, 2004); and (ii) direct volcanic supply. Mutual eclipses between Io and other Galilean satellites (Schneider *et al.*, 1991; Burger *et al.*, 2001) have allowed observations of Io's corona down to $\sim 1.4 R_{Io}$ and radial profiles of the

Na column density to be derived. The Na corona appears denser on the sub-Jupiter compared with the anti-Jupiter side, with an average radial profile $\mathcal{N}_{Na}(b) = 2.2 \times 10^{12} b^{-2.34}$ for $b > 1.5 R_{Io}$ (Burger *et al.*, 2001). Extrapolation of the profile down to the surface agrees reasonably well with an estimate ($\mathcal{N} \sim 4 \times 10^{12} \text{ cm}^{-2}$) based on the detection of Na emission in Jupiter eclipse, probably excited by torus electrons (Bouchez *et al.*, 2000). Based on *Galileo* images, Burger *et al.* (1999) identified a fast sodium jet with a source region much smaller than Io, perhaps confined to volcanically active regions. Potassium measurements have been made down to $\sim 10 R_{Io}$, giving column densities at that distance of $\sim (0.4-1.5) \times 10^9 \text{ cm}^{-2}$, and the Na/K ratio was derived and shown to be constant from 10–20 R_{Io} at a value of 10 ± 3 (Brown, 2001).

O, S, Na, K, and Cl emissions, produced by collisional excitation of neutrals in the atmosphere and corona by torus electrons, have also been detected. Though richly documented (e.g., Oliverson *et al.*, 2001), these atomic emissions are not straightforward to interpret in terms of atmospheric properties for a variety of reasons, particularly because the observed brightnesses are diagnostic of both the neutral densities and plasma conditions, and because the predominant excitation mechanism (direct excitation of atomic species or molecular dissociative excitation) is uncertain. Assumptions and simplifications have to be made, and forward modeling, as opposed to inversion, is generally the most successful approach. Nonetheless, these observations have provided valuable constraints on the nature of the atmosphere and its composition. Regarding sodium, an exciting recent development (Mendillo *et al.*, 2004; Wilson *et al.*, 2002) exploits observations of the extended Na nebula to show that the shape and brightness of this cloud is determined by the mechanism and rate of Na escape, and is correlated with the infrared activity level of Io (known to be indicative of volcanic activity, particularly lava flows). Wilson *et al.* (2002) argue that this provides evidence that escape of material from Io's atmosphere occurs predominantly from collisionally thick regions rather than from the exosphere.

Atomic sulfur and oxygen have been observed extensively both in the plasma torus since 1981 (Brown, 1981; Durrance *et al.*, 1983; see Chapter 11), and near Io since 1986 (Ballester *et al.*, 1987). A common, albeit rough, approach to interpretation of the near-Io observations has been to assume electron excitation of the atomic species, and constant electron density (n_e) and temperature (T_e) along the line-of-sight. From disk-average *IUE* spectra, and assuming canonical torus values of $T_e = 5 \text{ eV}$ and $n_e = 2,000 \text{ cm}^{-3}$, Ballester (1989) inferred minimum oxygen column densities of $\mathcal{N}_O > (4-7) \times 10^{13} \text{ cm}^{-2}$. Limits on the sulfur column density of $2.2 \times 10^{12} \text{ cm}^{-2} < \mathcal{N}_S < 7 \times 10^{15} \text{ cm}^{-2}$ were also derived. In the spatially resolved spectroscopic observations of McGrath *et al.* (2000) described earlier, emission from the SI] 1900,1914 Å doublet was detected over Pele and T3, and the sulfur column density above Pele was estimated to be $\mathcal{N}_S \sim 1 \times 10^{14} \text{ cm}^{-2}$. From HST/STIS data resolving the 1,479 Å multiplet, Feaga *et al.* (2002) obtained an improved determination of the S tangential column density, independent of electron density and temperature, and found it to be $3.6 \times 10^{12} \text{ cm}^{-2} < \mathcal{N}_S < 1.7 \times 10^{14} \text{ cm}^{-2}$ (as revised by McGrath *et al.* (2004); the vertical column density is a factor of ~ 7 lower). Spatial profiles of SI] and OI] emissions with a

resolution of $\sim 0.05 R_{\text{Io}}$ out to distances of $\sim 10 R_{\text{Io}}$ were determined by Wolven *et al.* (2001). Though these intensities vary considerably with System III longitude, probably in response to varying local electron density, the ratio of the sulfur to oxygen emission is fairly constant in time and with distance from Io.

Monochromatic (HST) and eclipse broadband (*Galileo*/SSI and *Cassini*/ISS) images have revealed a complex morphology of the atomic emissions, characterized by five notable features: equatorial "spots", volcanic plume glows, a limb-brightened ring of emission just off the disk, diffuse atmospheric emissions (also referred to as "glow"), and emission from Io's extended corona. The spots (often referred to as the "Io aurora") are brightest along the equator and near the sub-Jupiter and anti-Jupiter points. They are observed to rock about the equator in concert with the changing orientation of the background Jovian magnetic field, constraining the electrodynamic interaction between plasma and satellite (Saur *et al.*, 2000; Saur and Strobel, 2004; see below). The limb-brightened rings of sulfur and oxygen emission imply that both species form global components of the atmosphere.

In the *Galileo*/SSI images of Io taken during 14 eclipses over 1996–1998 (Geissler *et al.*, 1999; see Chapter 8) equatorial spots are seen in all filters, but most prominently in the violet, while the diffuse glow is detected in the green filter. The identity of the emitters cannot be unambiguously determined, however, several candidates were proposed by Geissler *et al.*, including [OI] 6,300 and 6,363 Å, H α 6,563 Å, and SII 6,720, 6,730 Å in the red filter; [OI] 5,577 Å and NaI 5,889, 5,896 Å in the green filter; and molecular emission from SO₂ in the violet filter. The likely role of oxygen in the SSI red filter, of sodium in the green, and of SO₂ (or SO) continuum emission in the violet was confirmed by the high spectral resolution observations of Bouchez *et al.* (2000), who detected auroral emission from [OI] 6,300, 6,363, 5,577 Å and Na 5,889, 5,896 Å, but no emission in the SSI violet region. This is also consistent with the detection of the equatorial glows in near-ultraviolet *Cassini*/ISS images (Geissler *et al.*, 2004), whose narrow filters compared with *Galileo* reduced the ambiguity in emitter identification, and which, in addition, confirmed a much larger vertical extent of the O emissions (up to 900 km) compared with the SO₂, confined near the surface. Additional emissions, in the 730–800-nm and 390–500-nm ranges, were attributed to atomic potassium and molecular disulfur (S₂), respectively.

The evolution of the atomic emissions shortly before, after, and during eclipses potentially provides a powerful diagnostic of the sources, nature, and stability of Io's atmosphere. Disk-averaged observations of Io passing into Jupiter shadow (Clarke *et al.*, 1994) showed that the far-ultraviolet sulfur and oxygen emissions decreased by a factor of ~ 3 within 20 min of Io entering eclipse. In contrast, Geissler *et al.* (1999) report an increase of the plume glows in a comparison of images obtained 11 min after the start of an eclipse and 41 min later. A dramatic, factor-of-2, increase in the S and O emission brightnesses was observed from HST/STIS in February 2000 by Wolven *et al.* (2001) when Io emerged into sunlight after eclipse, and interpreted as the recovery of a sublimation-supported SO₂ atmosphere. Retherford (2002) quantified these changes for the spots, the limb glow, and the extended corona, and estimated that the collapse timescales for the molecular atmosphere, atomic atmosphere, and corona after ingress are ~ 5 min, ≤ 30 min (conservatively), and ~ 280 min (i.e., longer than the

duration of an eclipse) respectively, consistent with the STIS eclipse observations. Geissler *et al.* (2004) showed evidence for a longer timescale for ingress dimming compared with egress brightening, from which they concluded that partial atmospheric collapse occurs, although the persistence of the equatorial aurora throughout eclipse indicates the existence of a volcanically supported component. Saur and Strobel (2004) developed an electrodynamic interaction model to interpret these results. Though seemingly intuitive, the decrease of the far-ultraviolet emissions upon eclipse entry is in fact not straightforward because far-ultraviolet intensities do not vary monotonically with the SO₂ column densities, as too dense an atmosphere will limit the atmospheric penetration of the electrons. A maximum of the far-ultraviolet emission typically occurs for column densities of $\sim 2 \times 10^{14} \text{ cm}^{-2}$. Saur and Strobel (2004) modeled the evolution of radiation in eclipse and found that the non-condensable atmospheric component must remain below $\sim (3-5) \times 10^{14} \text{ cm}^{-2}$; otherwise, the emissions would *brighten* during eclipse. They further show that the existence of equatorial spots throughout eclipse, as observed by Geissler *et al.* (2004), provides a *lower limit* to this component of $\sim (3-5) \times 10^{14} \text{ cm}^{-2}$. While the coincidence with the upper limit may be somewhat accidental, the combination of the two provides a tight constraint on the volcanic component. Saur and Strobel (2004) conclude that sublimation dominates over volcanic emission by at least an order of magnitude in maintaining the SO₂ atmosphere. Finally, the post-eclipse growth of the Na fluorescent emission was recently studied by Morgan *et al.* (2004). They found that, as time passes after eclipse, sodium, initially confined to large distances from Io, progressively increases in the vicinity of Io. This was interpreted as due either to re-exposure of surface sodium to sputtering due to sublimation of SO₂ condensed during eclipse, or to a temperature dependence of the sputtering process.

The detections of Cl ions in the plasma torus (Kueppers and Schneider, 2000; Feldman *et al.*, 2001) and of NaCl in the atmosphere have motivated searches for atomic chlorine in Io's bound atmosphere. Using spatially resolved HST/STIS spectral images, Retherford (2002) identified Cl emission at two wavelengths in the equatorial spots, at a relative abundance ratio of Cl/O $\sim 0.07-1\%$. Feaga and McGrath (2004) used archival disk-averaged HST/GHRS data acquired over 1994-1996 to detect two Cl multiplets, and inferred self-consistent relative ratios of chlorine, sulfur and oxygen, namely Cl/O = 0.017 ± 0.008 , Cl/S = 0.1 ± 0.05 , and S/O = 0.18 ± 0.08 . They also find evidence for large temporal variations of the chlorine emission, which supports a volcanic origin for NaCl.

10.2.4 Ionosphere

As mentioned above, the interpretation of the initial detection of Io's ionosphere by *Pioneer 10* met only limited success. Since then, results from a series of six *Galileo* radio occultation measurements in 1997 (Hinson *et al.*, 1998) have greatly clarified the situation. A first important point is that the viewing geometry in radio-occultations always puts both the entrance and exit measurements within a few degrees of the terminator. As a result, both measurements primarily sample the sunlit atmosphere, as even when they occur above the night-time terminator, only the lower few kilometers

of the atmosphere are in darkness. Thus, the *Galileo* occultations in fact sampled a wide variety of geometries of the sunlit hemisphere relative to the plasma ram direction, yielding information on the distribution and motion of the plasma near Io. The plasma distribution shows two components. The first is present within a few hundred kilometers of Io's surface throughout the upstream and downstream hemispheres and resembles a bound ionosphere. Vertical electron density profiles for this component were derived at 10 locations near Io's terminator. The peak density exceeded $5 \times 10^4 \text{ cm}^{-3}$ at 9 out of 10 locations, with a maximum of $2.8 \times 10^5 \text{ cm}^{-3}$. The peak density varied systematically with Io longitude, with maxima near the centers of the sub- and anti-Jovian hemispheres (i.e., in correspondence with the auroral glows seen in eclipse), and minima near the centers of the downstream and upstream hemispheres. This pattern may be related to the Alfvénic current system induced by Io's motion through the magnetospheric plasma. The vertical extent of the bound ionosphere increases from ~ 200 km near the center of the upstream hemisphere to ~ 400 km near the boundary between leading and trailing hemispheres.

The second component is highly asymmetric, consisting of a wake that appears only on the downstream side and extends to distances as large as $10 R_{\text{Io}}$. Plasma near Io's equatorial plane was measured to move from Io in the downstream direction, with velocity increasing from 30 to 57 km s^{-1} from 3 to 7 Io radii. The latter velocity corresponds to corotation, suggesting that bulk plasma motion was being observed. From the entire data set, it appears that the major factor determining the morphology of the ionosphere is the plasma ram direction. The *Galileo* measurements generally confirm the original *Pioneer 10* results, providing strong evidence that the ionosphere is stable. They also demonstrate that the *Pioneer 10* entrance profile was dominated by wake electrons, which in retrospect explains the inability of the 1-D photochemical models to match this profile.

10.3 RECENT MODELING DEVELOPMENTS

As outlined in the introduction, studies of Io's atmosphere were largely dominated by modeling in the 1980–1990 decade. Because of the complexity of the Io surface/atmosphere/ionosphere/plasma torus system, most modeling work has focused on single aspects of the problem, such as the atmospheric vertical structure, its photochemistry, its horizontal distribution, or its interaction with the plasma torus. The wealth of new data acquired in the last 15 years prompted a reassessment of most of these “single aspect” models. Additionally, they justified the development of more elaborate, multi-dimensional, “unified” models. We now review these recent modeling efforts.

10.3.1 Modern buffered models

The early ultraviolet observations of Ballester *et al.* (1990, 1994) motivated Kerton *et al.* (1996) to reconsider the sublimation equilibrium models of Fanale *et al.* (1982) which gave SO_2 abundances larger than the observed SO_2 abundances or upper limits.

The Kerton *et al.* models rectified some of the oversimplifications in the treatment of surface radiative equilibrium by including a variety of physical processes previously ignored: latent heat of SO₂ frost sublimation, thermal conduction, diurnal rotation, internal heat flow, and deposition of solar energy below the surface (“solid-state greenhouse effect”). Results of these improved models, expected to give a more accurate representation of Io’s surface temperatures and hence equilibrium pressures, differ from the early picture in several ways. First, the surface temperature and pressure gradients toward the periphery of Io’s disk are much more gradual than in the standard equilibrium models. Second, the surface temperature distribution is no longer symmetric about the subsolar point, since accounting for heat conduction shifts the maximum temperature slightly from the subsolar point toward the dusk terminator. These improvements result in reduced column abundances, more consistent with the Ballester *et al.* (1994) results. Note however that some model parameters, such as the frost albedo, the thermal conductivity, and the efficiency of subsurface greenhouse, are uncertain, so a range of SO₂ distributions remains possible. In the most extreme cases (the high-conductivity C/R/L model, their Figure 6, and the subsurface greenhouse model, their Figure 8), the SO₂ pressure near the poles is many orders of magnitude lower than near the terminators, which is qualitatively consistent with interpretations of the Ly α images (Feldman *et al.*, 2000; Strobel and Wolven, 2001; Feaga *et al.*, 2004).

10.3.2 Volcanic gas composition models

The continuous improvement of our knowledge of the atmospheric composition, and in particular, the gaseous plume composition information now available for Pele, prompted the development of thermo-chemical models of Ionian volcanic gas chemistry (Zolotov and Fegley, 1998a, 1998b, 1999, 2000; Fegley and Zolotov, 2000; Schaefer and Fegley, 2005). By analogy with volcanic eruptions on Earth where gases erupted at temperatures ≥ 900 K are hot enough for thermo-chemical equilibrium, the basic idea of these models is that eruption temperatures on Io – measured to range up to 1,700 K – are high enough that volcanic gases chemically equilibrate in the vent vicinity during eruptions. In contrast, volcanic gases are assumed to be quenched in the cooling expanding plumes. Inputs to the models are the eruption temperature, total pressure, and bulk elemental composition of the volcanic gases. This kind of model allows one to calculate an atmospheric composition as a function of the eruption conditions, or, vice versa, to use a measured (global or local) composition to infer physical and chemical conditions in the erupting magma (in particular the oxidation state) as well as information on the vent pressure. The major results of these models are summarized below.

Zolotov and Fegley (1998a) show that SO is a natural product of thermodynamical equilibrium in erupted materials, and that the observed SO/SO₂ mixing ratio (3–10%) can be fit for suitable combinations of gas pressure, temperature, and O/S < 2 ratio at the vent. Zolotov and Fegley (1998b) further predict S₂O to be an important volcanic species, reaching 1–6% of SO₂ in the vicinity of SO₂–S₂ vents erupting from magmas of 1–100 bar total pressure. Regarding sodium and alkalis, NaCl is the

expected dominant Na- and Cl-bearing volcanic gas for high-temperature ($>1,400$ K) eruptions (Fegley and Zolotov, 2000). Its abundance is expected to reflect the elemental Cl/S in the erupting magmas and is nominally predicted to be 4%. The lower abundance measured by Lellouch *et al.* (2003), 0.3–1.3% in the “volcanic models”, appears in fact more consistent with a chondritic composition (having Cl/S = 0.01), a surprising result given that higher Na/S and Cl/S are expected in Io's lithosphere due to igneous differentiation. Alternate explanations for the low apparent NaCl/SO₂ ratio are discussed by Lellouch *et al.* (2003). Fegley and Zolotov further predict a suite of Cl- and K-bearing molecular species, including notably KCl, (NaCl)₂, SCl₂, and S₂Cl. The list of potential molecules was recently extended to other alkali and halogen species, including Rb, Cs, F, Br, and I compounds (Schaefer and Fegley, 2005). Finally, Zolotov and Fegley (2000) used the observed SO₂–SO–S₂–S Pele plume composition (Spencer *et al.*, 2000; McGrath *et al.*, 2000) to present a detailed chemical model for the plume. Though, given Pele's known variability, it is risky to fold data taken 3 years apart into a single plume model, this approach suggests an $\sim 10^{-5}$ -bar pressure in the vicinity of the vent, and implies that the Pele plume gas last equilibrated at magmatic temperature and was not significantly altered in the eruption. The composition of the Pele plume does indicate that Io is differentiated, and that metallic iron and free carbon are not abundant in bulk silicates on Io.

10.3.3 Radiative models

Radiative models are concerned with calculations of the atmospheric vertical (temperature and density) profile from an analysis of the heat budget. Most of these models were developed in 1-D and for the case of a pure SO₂, hydrostatic, atmosphere. Strobel *et al.* (1994) developed the first comprehensive model of Io's vertical thermal structure, extending and improving upon the models by Kumar (1985) and Lellouch *et al.* (1992). They solved the time-dependent, 1-D heat balance equation with heat transport by diffusive and radiative processes. Heating sources include solar heating in the ultraviolet and near-infrared bands of SO₂, as well as plasma and Joule heating. Radiative losses are due to non-LTE cooling by SO₂ rotational and vibrational lines, for which a new and elaborate treatment was developed. Two cases were considered in the Strobel *et al.* models, a high-density atmosphere representative of the (smaller fractional coverage, larger column abundance) regime typified by the early interpretation of the millimeter observations, and a low-density atmosphere intended to represent the (larger fractional coverage, lower column abundance) regime typified by the early disk-averaged ultraviolet observations (Figure 10.6). Their model predicts the existence of a mesopause in Io's atmosphere when the surface pressure exceeds ~ 10 nbar, as already noted by Lellouch *et al.* (1992). With a lower scale height temperature consistently below 200 K, none of the model atmospheres generated with solar heating only were hot enough to satisfy the hydrostatic interpretation of the millimeter data, nor the bulk atmospheric temperature of 200–400 K derived from the ultraviolet data. Plasma heating, associated with impacting thermal ions from the Io plasma torus as they sweep by Io's exosphere/upper atmosphere (Johnson, 1989), and Joule heating, driven by the penetration of Jupiter's

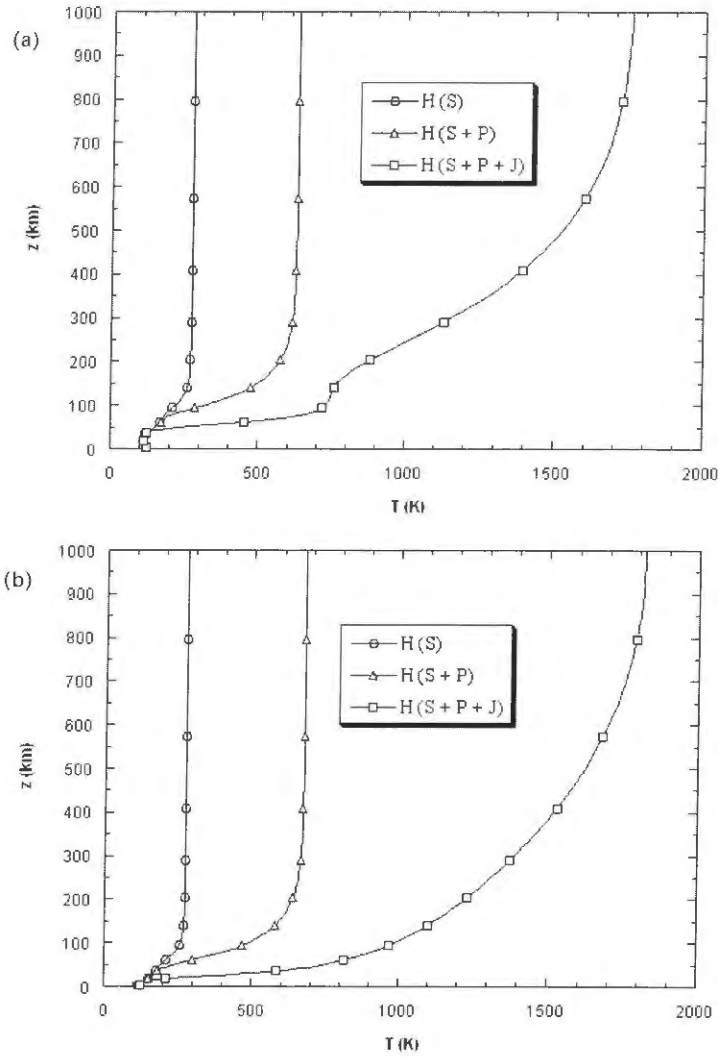


Figure 10.6. Effects of solar (S), solar + plasma (S + P), and solar + plasma + Joule (S + P + J) heating on the vertical thermal structure of Io's atmosphere. (a) Surface pressure = 130 nbar. Note the presence of a mesosphere. (b) Surface pressure = 3.5 nbar (from Strobel *et al.*, 1994).

corotational electric field into Io's conducting ionosphere, can raise the atmospheric temperature considerably (up to 1,800 K). However, unless it penetrates significantly below the exobase, plasma heating primarily elevates the exospheric temperature. Joule heating can in principle produce an atmosphere with a bulk temperature greater than 200 K, but only for surface pressures in the range 0.1–1 nbar, so that none of the models appears warm enough to satisfy the hydrostatic interpretation of the early millimeter observations. Strobel *et al.* (1994) also established that radiative time

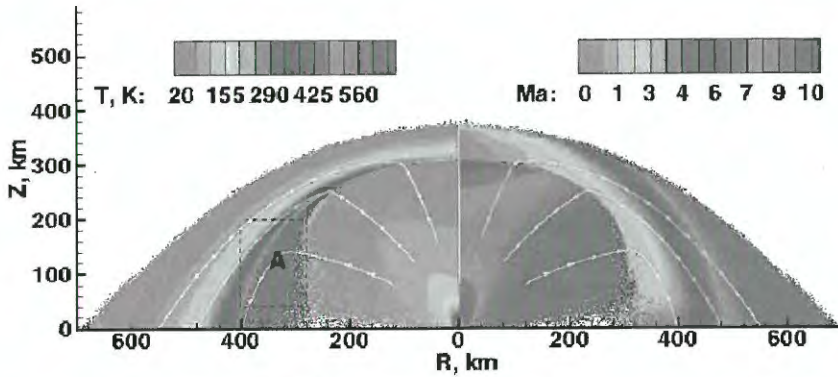


Figure 10.7. Model of an isolated Pele-type volcanic plume. Contours of the temperature and Mach number are shown (from Zhang *et al.*, 2003). (See also color section.)

constants are short (~ 20 min in the mesosphere and ~ 1 hr in the thermosphere), competitive with dynamical timescales.

Recently, thermal calculations have been extended to plume atmospheres (see extended discussion in Chapter 8). These complex models (Zhang *et al.*, 2003) consist of Monte Carlo simulations of gas dynamics and describe phenomena such as plume expansion and re-entry shock, including the effect of radiative cooling. They consider the case of nightside isolated plumes, and the case of dayside plumes erupting in a background atmosphere. Figure 10.7 shows model results for gas temperature and Mach number for the case of an isolated Pele-type plume. Such models show interesting features, such as multiple bounce shock structure around Prometheus-like plumes (not shown in the example of Figure 10.7), or the depletion of frost on the dayside from plume erosion. Venting rates needed to sustain the observed column densities are estimated. In a more recent study, Zhang *et al.* (2004) modeled the entrainment of particulates in the gas flow, and were generally successful at reproducing the plume structures, shadows, brightness distribution, and deposition patterns observed in the *Voyager* and *Galileo* images. Based on the lateral extent of some plumes, and the absence of observable dust clouds (which constrains dust settling times), they inferred constraints on the density of the background sublimation atmosphere, for which they found an equilibrium temperature in the range 110–118 K. In most of the Zhang *et al.* (2003, 2004) models, number densities in the vent vicinity reach $5 \times 10^{11} \text{ cm}^{-3}$, for a column density of $\sim 10^{18} \text{ cm}^{-2}$ within ~ 20 km of the vent. Column densities averaged over the plumes are in reasonable agreement with the volcanic atmosphere interpretation of the millimeter and $\text{Ly}\alpha$ data (Lellouch, 1996; Strobel and Wolven, 2001).

10.3.4 Photochemical models

Photochemical models of Io's atmosphere, also mostly developed in the context of 1-D hydrostatic atmospheres, aim at predicting an equilibrium atmospheric composi-

tion. Making use of the thermal structure of Strobel *et al.* (1994), Summers and Strobel (1996) focused renewed effort on the photochemical modeling in order to gauge the sensitivity of the chemical structure to vertical transport rates, and to evaluate the possibility that O₂ and/or SO may be significant dayside or nightside constituents. Unlike the earlier photochemical models, they tested both low and high values of the eddy mixing rate. Their results confirmed the prediction (Kumar, 1985) that SO is an important atmospheric constituent. Comparing the SO/SO₂ mixing ratio derived from the millimeter observations with the Summers and Strobel (1996) model, in which SO is assumed to be lost at maximum diffusive rates to the surface and the exobase, indicates an effective vertical eddy diffusion coefficient K in the range 3×10^6 to $3 \times 10^7 \text{ cm}^{-2} \text{ s}^{-1}$. This is much less than estimated by Summers and Strobel from a dimensional analysis of Ingersoll's (1989) model of regional frost patch control, which gives $K \sim 10^9 \text{ cm}^{-2} \text{ s}^{-1}$. Another way of looking at the problem is to note that, with typical SO₂ column densities of $(1-4) \times 10^{33}$ molecules on a hemisphere, and a SO₂ photolytic rate of $\sim 8 \times 10^{-6} \text{ s}^{-1}$, the SO hemispheric production rate is $(0.8-3.2) \times 10^{28} \text{ s}^{-1}$, which must be balanced by transport. For a hydrostatic atmosphere, considering vertical eddy, vertical molecular, and horizontal transport, a characteristic transport time of 10^4 s can be assumed. This leads to a hemispheric average of $(4-16) \times 10^{14} \text{ cm}^{-2}$ SO molecules, in agreement with observations. In contrast, for photolysis in a plume atmosphere, the flight time is only 500–1,000 s, and the mechanism seems to fail by a factor of 5–10. Thus, if Io's atmosphere is in dynamical equilibrium with volcanic sources rather than hydrostatic, the origin of SO may be thermo-chemical rather than photochemical.

While the Summers and Strobel (1996) calculations included several minor molecular Na species, none of the cases considered could simultaneously produce the large atomic and molecular Na escape rates of Wilson and Schneider (1994) and Smyth and Combi (1988) and provide a good match to the *Pioneer 10* ionospheric profile. Finally, although the production of a tenuous molecular oxygen atmosphere from SO₂ photolysis was confirmed, Summers and Strobel found that the fast reaction between S and O₂ severely limits the O₂ column density to much lower levels (10^{-4} times) than calculated by Kumar and Hunten (1982).

Moses *et al.* (2002a,b) have revisited the 1-D aeronomic models in order to address how active volcanism might affect the standard picture of photochemistry on Io. Although still based on a static atmospheric structure, these models study the photochemistry of an atmosphere compositionally enriched by volcanic emissions, as described for the Pele-type eruptions by the thermo-chemical equilibrium calculations discussed above. The models address the effects of photolysis, chemical kinetics, condensation, and vertical eddy and molecular diffusion on the subsequent evolution of the volcanic gas. The first paper focuses on sulfur and oxygen species. As might be expected, if S₂ is a common volcanic gas, the sulfur species (S, S₂, S₃, S₄, SO, and S₂O) are enhanced relative to the oxygen species (O and O₂), as compared with frost sublimation (i.e., initially SO₂-only) models. Possible variations in the SO/SO₂ ratio, tentatively reported by McGrath *et al.* (2000), may reflect the spatial and temporal variability of volcanic SO. Many of the volcanic species (S₂, S₃, S₄, and S₂O) are short-lived (from minutes to a few hours at the most), due to

condensation or photolytic loss, so these species are expected to be rapidly removed from the atmosphere once volcanic plumes are shut off. Their second paper extends the study to alkali and chlorine species, for which it is predicted that NaCl, Na, Cl, KCl, and K are the dominant species generated from Pele-type eruptions, for a wide range of conditions. Again, these species all have short atmospheric lifetimes, so their presence implies continuous volcanic output. The Moses *et al.* (2002b) study further shows that even if molecular NaCl dominates in the lower atmosphere, atomic Na and Cl are respectively the major Na- and Cl-bearing species at the exobase. The upward flux of NaCl at the top of the atmosphere is only $\sim 0.1\%$ of the upward (volcanic) flux at the bottom; the corresponding atomic Na and Cl flux at the top are ~ 10 – 20 times larger. Combined with the NaCl volcanic emission rates measured by Lellouch *et al.* (2003), this indicates escape fluxes of 2×10^{25} to 2×10^{26} Na and Cl atoms per second. This range is consistent with estimates of the supply rate of low-speed sodium in the neutral clouds, and with the production rate of the molecular ions (NaX^+) invoked to explain the high-velocity Na^* features. As the Cl/S and Na/S ratio in the torus are comparable ($\sim 2\%$), Lellouch *et al.* (2003) conclude that: (i) NaCl is the common parent of sodium and chlorine in Io's environment, mostly through escape of photolytically produced Na and Cl; and that (ii) unless plume dynamics preferentially enhance the escape of molecular NaCl, the production of fast sodium is not dominated by direct ionization of NaCl, but rather by reactions of atomic Na with other torus molecular ions.

10.3.5 “Unified” models

Although models have yet to capture the full complexity of Io's atmosphere, first steps have now been taken to combine descriptions of the vertical structure, horizontal transport, and photochemistry. In a series of papers (Wong and Johnson, 1995, 1996; Wong and Smyth, 2000; Smyth and Wong, 2004), Wong and co-workers attempted to predict, in the framework of a sublimation driven hydrostatic SO_2 atmosphere axisymmetric about the subsolar point, the 2-D atmospheric structure, including composition, as a function of altitude and SZA. Unlike the plume atmosphere models mentioned above, which use a direct simulation Monte Carlo (DSMC) method, the Wong and co-workers' simulations use a continuum fluid model. The first paper focused on the effect of plasma heating on the sublimation-driven flow of an SO_2 atmosphere. It was found that plasma heating is most important near the exobase, raising the exobase altitude and the fraction of the surface over which the atmosphere is collisionally thick, with implications for the supply to the torus. Joule heating, radiative cooling, vertical transport, and photochemistry, were all included in the model of Wong and Johnson (1996), which was mainly concerned with SZA variations, and in particular the possibility that non-condensable species (O_2 and possibly SO) could accumulate, dominate the atmospheric dynamics, and build up on the nightside. They found, in particular, that the build-up of a nightside atmosphere does not suppress the dayside-to-nightside atmospheric flow but reduces it, and raises the overall atmospheric pressure. Wong and Smyth (2000) extended these calculations to high- and low-density SO_2 atmospheres at both

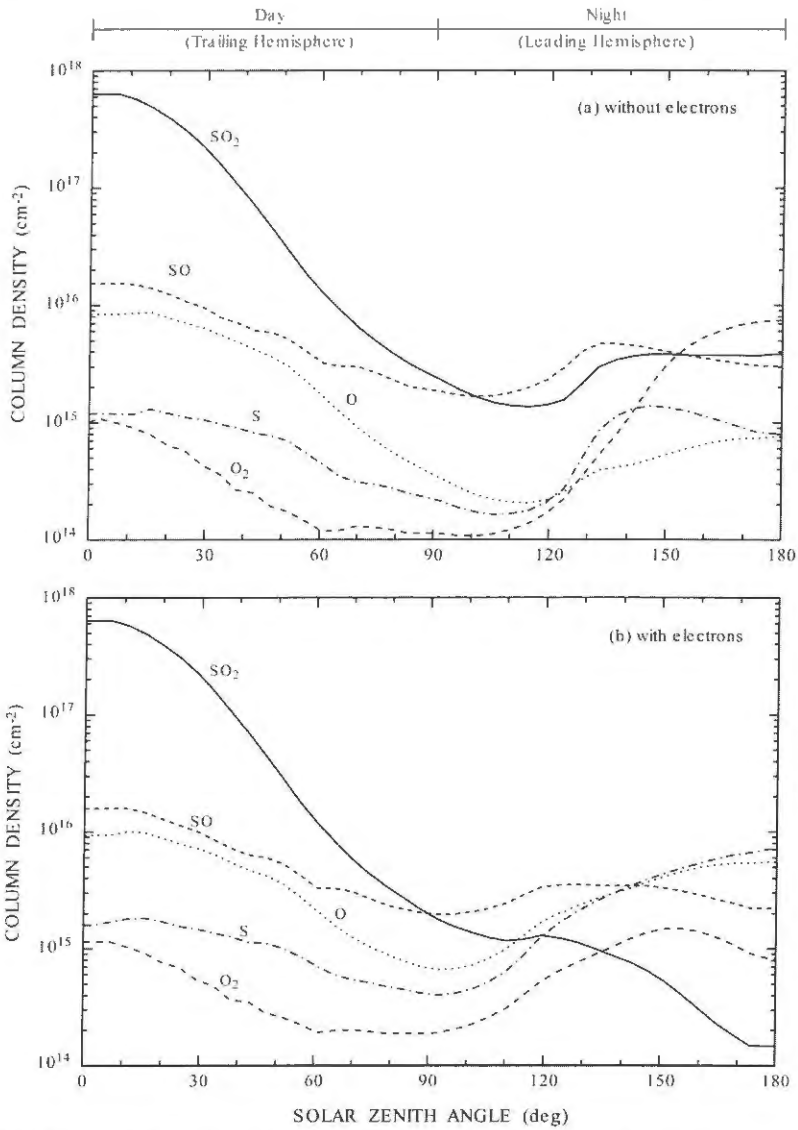


Figure 10.8. Impact of electron chemistry on neutral column densities in Io's atmosphere. Calculations apply to a sublimation atmosphere with a subsolar surface temperature of 120 K at western elongation (from Smyth and Wong, 2004).

western and eastern elongation, using an updated version of the multispecies hydrodynamic code, including an updated treatment of plasma heating, as well as simple Na chemistry. Assuming that O₂ and SO are both non-condensable, they find that gas-phase reactions between them can produce a substantial amount of SO₂ in the nightside atmosphere. These calculations also illustrate a huge variability of the

exobase altitude and temperature as a function of SZA. Different SZA-dependences of the pressure and composition occur at eastern and western elongation, as a consequence of the plasma energy being added to the dayside (western) or nightside (eastern) hemisphere. The calculations achieve a 3–7% SO/SO₂ mixing ratio on the dayside, consistent with observations. They also predict substantial amounts of O₂ and SO on the nightside, typically 10¹⁵ cm⁻² or more. This is at odds with the results of Summers and Strobel (1996) and results from the assumption that SO is non-condensable. Most recently, Smyth and Wong (2004) modeled the impact of electron chemistry on the atmospheric composition and structure. Being confined to an interaction layer at column densities of several 10¹⁵ cm⁻², electron chemistry is important primarily only on the nightside. There, compared with the model of Wong and Smyth (2000), SO₂ is drastically reduced, SO and O₂ are significantly reduced, and S and O are dramatically enhanced to become the dominant species (Figure 10.8).

10.4 SYNTHESIS AND PROSPECTS

10.4.1 The emerging picture

Data obtained since 1990 reach a number of reassuringly consistent conclusions, the most prominent of which being that Io's SO₂ atmosphere is tenuous but well collisionally thick, permanently detectable on both its leading and trailing dayside hemispheres, and relatively stable, with only limited variability observed to date. This readily excludes the purely subsurface cold trap and purely sputtered models. Furthermore, the ensemble of data gives direct evidence for a generally widespread atmosphere, but with significant horizontal variations in pressure. These variations consist of: (i) modest (at the resolution of the measurements (i.e., ~200 km at best)) local density enhancements over active plumes at low- to mid-latitudes; (ii) longitudinal variations of the SO₂ column density in the equatorial region, with a maximum on the anti-Jupiter hemisphere, perhaps by a factor as much as 10; and (iii) a general decrease of the gas pressure with increasing latitude, rather smooth in tropical regions, but probably sharp at latitudes above ±45°. These features are consistent with most of the ultraviolet and infrared measurements, which converge to indicate mean column densities of ~ (1–5) × 10¹⁶, covering typically 50–70% of Io's dayside atmosphere, mostly but not exclusively at low latitudes.

Although the distribution of Io's atmosphere is too complex to be accurately characterized by a single phrase such as “patchy” or “extended”, this emerging picture generally favors the (larger surface coverage, smaller column abundance) regime as opposed to the (smaller surface coverage, higher column abundance) regime. This contradicts the initial interpretation of the millimeter-wave observations, which depicted Io's atmosphere as confined to a very small (<10%) fraction of the surface. Better agreement is achieved with the “volcanic model” interpretation of these data, in which the extremely patchy character of the atmosphere can be relaxed. This latter interpretation is thus preferable, although it requires the difficult-to-assess scenario in which the atmosphere results from direct output from tens to hundreds of

volcanic centers. Taking published numbers at face value, a severe discrepancy remains with the *Galileo*/ultraviolet spectrometer (UVS) data which invoked very high column densities. Reconciliation may be possible if the broadband structure seen in the UVS data is due to surface materials rather than SO₂ gas, and/or if very dense patches are smaller than the ~200-km resolution of the Ly α images (see McGrath *et al.*, 2004). Except for the initial *Voyager*/IRIS measurement, and for which the SO₂ abundance has been revised downwards, there is in fact little compelling observational evidence for very large localized enhancements. This, however, may be the result of insufficient spatial resolution, as both the “averaging length” estimate of Ingersoll (1989) and the detailed calculations of Zhang *et al.* (2003) suggest that an order-of-magnitude decrease of the column density occurs within a few tens of kilometers of plume centers.

10.4.2 The volcanic vs. sublimation nature of Io’s atmosphere

Trying to settle the “essential” question that arose after the initial discovery of SO₂ in Io’s atmosphere remains risky, and Io’s atmosphere seems to express a dual nature. We first stress that while active volcanism has long been recognized to be the ultimate source of Io’s atmosphere (e.g., Ingersoll, 1989), the question of whether its immediate source is sublimation or volcanic venting is significant, in terms of vertical structure, thermal structure, lifetime, response to insolation variations, and composition, as amply illustrated by the recent models.

The bulk features of Io’s atmosphere, as summarized above, are in fact consistent both with sublimation equilibrium and with a volcanic maintenance of the atmosphere. A typical column density of $3 \times 10^{16} \text{ cm}^{-2}$ (i.e., a mean pressure of 0.6 nbar), is consistent with a sublimation temperature of 112 K or, equivalently (rescaling from Ingersoll, 1989) a total volcanic source of $\sim 30 \text{ ton s}^{-1}$. As pointed out by Spencer *et al.* (2005), the longitudinal distribution of SO₂, peaked on the anti-Jovian hemisphere, is consistent with the *Galileo*-derived maps of the SO₂ frost distribution (Douté *et al.*, 2001), which indicate that SO₂ frost is nearly ubiquitous on Io, but most abundant on the anti-Jovian hemisphere. However, the same is true for active volcanic plumes (Lopes-Gautier *et al.*, 1999), and in general regions of high frost content correlate well with plume longitudes. Unlike most active plumes, confined to tropical regions, SO₂ frost is present up to high latitudes. However, the lack of SO₂ gas poleward of $\sim 45^\circ$ does not argue for volcanic support, as it might just result from the surface temperature being too cold there.

Several observational results favor a predominantly sublimation-driven atmosphere. These include the relatively modest increase of the SO₂ pressure over active plumes (e.g., 40% only at Prometheus in the Jessup *et al.*, 2004a observations) and the fact that SO₂ gas has been detected at places where no active plume has even been observed (e.g., T3 in McGrath *et al.*, 2000). This may indicate an atmosphere globally sustained by sublimation, with only local enhancements due to volcanic output. The evolution of the far-ultraviolet/visible atomic features and the Na fluorescent emission during eclipse is generally consistent with sublimation/condensation processes. The interpretation by Saur and Strobel (2004) of this behavior assigns a minor role

($\leq 10\%$) to volcanic emissions in the direct maintenance of the SO_2 atmosphere as a whole.

Conversely, numerous observations favor the volcanic atmosphere concept. This includes: (i) the detection of SO_2 in the Pele plume at the terminator (i.e., in a place where the surface temperature is too cold for important sublimation to take place); (ii) the presence of species that have a negligible (NaCl , S_2) or uncertain (SO) vapor pressure; and (iii) the interpretation of the SO infrared observations in terms of hot excited SO directly emitted by Loki. These three results demonstrate that active plumes can directly inject measurable amounts of gases, although they do not explicitly address the question of the *spatial* extent of plume atmospheres and of the atmospheric control away from the visible plumes. To these relatively direct proofs, must be added a few circumstantial evidences. First, the fact that the "volcanic atmosphere" interpretation of the millimeter observations is to be preferred. In this respect, it must be noted that such "plume-like" models have not been applied to the analysis of other data. A second aspect is the apparent lack of diurnal variation in the $\text{Ly}\alpha$ images. This is a natural consequence of the volcanic model, although it can conceivably be accommodated by the sublimation model if the frost has a high thermal inertia. In the same spirit, the general lack of correlation between the infrared-derived column densities and heliocentric distance, except perhaps on the anti-Jupiter hemisphere, also tends to favor a direct volcanic support of the atmosphere. Albeit limited and insufficiently documented, the existence of temporal variability in the millimeter and some ultraviolet data sets may also be viewed in support of a volcanic atmosphere, since, with typical sublimating rates of 1 mm yr^{-1} and an SO_2 ice layer at least several centimeters thick (Schmitt *et al.*, 1994), a sublimation atmosphere is expected to be stable against short-term fluctuations. The correlation between the appearance and brightness of the extended sodium nebula with the IR activity level also points to a volcanic control of the atmosphere, although a mechanism by which lava flow would affect the atmosphere remains to be devised (Mendillo *et al.*, 2004). In addition to observations, the success of Zhang *et al.* (2003, 2004) in reproducing the mean gas density over the plumes as well as the general plume appearance, gives strong credit to the volcanic atmosphere concept.

10.4.3 Remaining uncertainties and future measurements

Future progress in our knowledge of Io's atmosphere will require further observations, some of which can be already identified. Local time vs. geographical effects must be disentangled in longitudinal variations, possibly by tracking a given region when it rotates from dawn to dusk. Abundance profiles must be determined systematically as a function of distance from volcanic centers, and individual volcanoes must be resolved.

The least well-constrained parameter in Io's atmosphere is the characteristic gas temperature T_{atm} . The Keck II observation of SO indicates that at least a fraction of the volcanic gas is hot (1,000 K) – implying that the thermodynamics of eruptive plumes are more complex than a mere adiabatic expansion. In the millimeter, the

hydrostatic interpretation of data from successive years has given contradictory results for T_{atm} (from 600–180 K), and the preferred volcanic interpretation does not constrain the gas temperature. In the ultraviolet, while many authors have simply assumed values for T_{atm} , the temperatures inferred by Ballester *et al.* (1994), McGrath *et al.* (2000), Spencer *et al.* (2000), and Jessup *et al.* (2004a, 2005) range from 110–500 K, with a general preference for 200–300 K. Though this problem is formidably difficult, especially for a volcanic atmosphere which is expected to exhibit huge lateral temperature variations, the determination of the characteristic temperature of the atmosphere and its variation with height should now be a priority. Local wind measurements would be of extremely high value in providing clues on local and global atmospheric dynamics. Current millimeter-data provide disk-averaged wind measurements, but their interpretation is uncertain (see McGrath *et al.*, 2004). Finally, observing the nightside molecular atmosphere would also provide very strong constraints on the atmospheric nature. Some of the above measurements can already be (or will soon be) performed from Earth or Earth-orbit, but several will require the operation of an Io orbiter.

From the theoretical/modeling point of view, efforts to link the different aspects addressed by current models should be undertaken. For example, while the “unified” models of Wong and co-workers address the coupling between vertical structure, planetary scale horizontal transport, and photochemistry, they do not include any description of volcanic plumes, and the validity of their continuum fluid model is uncertain in low-pressure regions. Conversely, while the Zhang *et al.* (2003, 2004) models may provide the most realistic description of the local structure of plume atmospheres, they do not provide a description of Io’s atmosphere as a whole, and additionally do not include any chemistry. Thermo-chemistry in volcanic gases is best depicted in the models by Zolotov and Fegley, but these models merely assume equilibrium near the vent source and instantaneous quenching well above the vent, without detailed consideration of interactions between the near-magma gas and the more extended volcanic atmosphere. The task of bringing these various pieces together promises to be formidable, but the success of the different models in their respective applicability fields seems to warrant the effort.

Io’s atmosphere, its apparent dual nature, and its interactions with the surface and the plasma environment, are clearly unique in the Solar System. Enormous progress in its knowledge has been achieved since our virtual state of ignorance at the end of the 1980s. Important questions do remain, but at least they seem to be now well posed, and a roadmap to solve them may be drawn.

10.5 REFERENCES

- Ballester, G. E. 1989. Ultraviolet observations of the atmosphere of Io and the plasma torus. PhD thesis, Johns Hopkins University, Baltimore, MD.
- Ballester, G. E., Moos, H. W., Feldman, P. D., Strobel, D. F., Summers, M. E., Bertaux, J.-L., Skinner, T. E., Festou, M. C., and Lieske, J. H. 1987. Detection of neutral oxygen and sulfur emissions near Io using IUE. *Astrophys. J.*, **319**, L33–L38.

- Ballester, G. E., Strobel, D. F., Moos, H. W., and Feldman, P. D. 1990. The atmospheric abundance of SO₂ on Io. *Icarus*, **88**, 1–23.
- Ballester, G. E., McGrath, M. A., Strobel, D. F., Zhu, X., Feldman, P. D., and Moos, H. W. 1994. Detection of the SO₂ atmosphere of Io with the Hubble Space Telescope. *Icarus*, **111**, 2–17.
- Belton, M. J. S. 1982. An interpretation of the near-ultraviolet absorption spectrum of SO₂. Implications for Venus, Io and laboratory measurements. *Icarus*, **52**, 49–165.
- Bouchez, A. H., Brown, M. E., and Schneider, N. M. 2000. Eclipse Spectroscopy of Io's Atmosphere. *Icarus*, **48**, 316–319.
- Bridge, H. S., Belcher, J. W., Lazarus, A. J., Sullivan, J. D., Bagenal, F., McNutt, R. L., Jr., Ogilvie, K. W., Scudder, J. D., Sittler, E. D., and Vasyliunas, V. M. 1979. Plasma observations near Jupiter: Initial results from Voyager 1. *Science*, **204**, 972–976.
- Broadfoot, A. L., Belton, M. J., Takacs, P. Z., Sandel, B. R., Shemansky, D. E., Holberg, J. B., Ajello, J. M., Moos, H. W., Atreya, S. K., Donahue, T. M. *et al.* 1979. Extreme ultraviolet observations from Voyager 1 encounter with Jupiter. *Science*, **204**, 979–982.
- Brown, R. A. 1974. Optical line emission from Io. In: A. Woszczyk and C. Iwaniszewska (eds), *Exploration of the Planetary System*. D. Reidel Publ. Corp., Dordrecht, The Netherlands, pp. 527–531.
- Brown, M. E. 2001. Potassium in Europa's atmosphere. *Icarus*, **151**, 190–195.
- Brown, R. A. 1981. The Jupiter hot plasma torus: Observed electron temperature and energy flows. *Astrophys. J.*, **244**, 1072–1080.
- Burger, M. H., Schneider, N. M., and Wilson, J. K. 1999. Galileo's close-up view of the Io sodium jet. *Geophys. Res. Lett.*, **26**, 3333–3336.
- Burger, M. H., Schneider, N. M., de Pater, I., Brown, M. E., Bouchez, A. H., Trafton, L. M., Sheffer, Y., Barker, E. S., and Mallama, A. 2001. Mutual event observations of Io's sodium corona. *Astrophys. J.*, **563**, 1063–1074.
- Cheng, A. F. and Johnson, R. E. 1989. Effects of magnetospheric interactions on origin and evolution of atmospheres. In: S. K. Atreya, J. B. Pollack, and M. S. Matthews (eds), *Origin and Evolution of Planetary and Satellites Atmospheres*. University of Arizona Press, Tucson, AZ, pp. 683–722.
- Clarke, J. T., Ajello, J., Luhmann, J., Schneider, N., and Kanik, I. 1994. Hubble Space Telescope ultraviolet spectral observations of Io passing into eclipse. *J. Geophys. Res.*, **99**, 8387–8402.
- De Pater, I., Roe, H. G., Graham, J. R., Strobel, D. F., and Bernath, P. 2002. Detection of the forbidden SO a¹Δ → X³Σ⁻ rovibronic transition on Io at 1.7 μm. *Icarus*, **156**, 196–301.
- Douté, S., Schmitt, B., Lopes-Gautier, N., Carlson, R., Soderblom, L., Shirley, J., and the Galileo NIMS Team. 2001. Mapping SO₂ frost on Io by the modeling of NIMS hyperspectral images. *Icarus*, **149**, 107–132.
- Durrance, S. T., Feldman, P. D., and Weaver, H. A. 1983. Rocket detection of ultraviolet emission from neutral oxygen and sulfur in the Io torus. *Astrophys. J.*, **267**, L125–L129.
- Fanale, F. P., Brown, R. H., Cruikshank, D. P., and Clark, R. N. 1979. Significance of absorption features in Io's IR reflectance spectrum. *Nature*, **280**, 760–761.
- Fanale, F. P., Banerdt, W., Elson, L., Johnson, T. V., and Zurek, R. 1982. Io's surface: Its phase composition and influence on Io's atmosphere and Jupiter's magnetosphere. In: D. Morrison (ed.), *Satellites of Jupiter*. University of Arizona Press, Tucson, AZ, pp. 756–781.
- Feaga, L. M., McGrath, M. A., and Feldman, P. 2002. The abundance of atomic sulfur in the atmosphere of Io. *Astrophys. J.*, **570**, 439–446.
- Feaga, L. M., McGrath, M. A., Feldman, P. D., and Strobel, D. F. 2004. Dependence of Io's SO₂ atmospheric column density on surface features. *Bull. Amer. Astron. Soc.*, **36**, 16.06.

- Feaga, L. M. and McGrath, M. A. 2004. Detection of atomic chlorine in Io's atmosphere with the Hubble Space Telescope GHRS. *Astrophys. J.*, **610**, 1191–1198.
- Fegley, B. and Zolotov, M. Y. 2000. Chemistry of sodium, potassium, and chlorine volcanic gases on Io. *Icarus*, **148**, 193–210.
- Feldman, P. D., Strobel, D. F., Moos, H. W., Retherford, K. D., Wolven, B. C., McGrath, M. A., Roesler, F. L., Woodward, R. C., Oliverson, R. J., and Ballester, G. E. 2000. Lyman- α imaging of the SO₂ distribution on Io. *Geophys. Res. Lett.*, **27**, 1787–1790.
- Feldman, P. D., Ake, T. B., Berman, A. F., Moos, H. W., Sahnou, D. J., Strobel, D. F., Weaver, H. A., and Young, P. R. 2001. Detection of chlorine ions in the *Far Ultraviolet Spectroscopic Explorer* spectrum of the Io plasma torus. *Astrophys. J.*, **554**, L123–L126.
- Geissler, P. E., McEwen, A., Ip, W., Belton, M. J. S., Johnson, T. V., Smyth, W. H., and Ingersoll, A. P. 1999. Galileo imaging of atmospheric emissions from Io. *Science*, **285**, 870–874.
- Geissler, P., McEwen, A., Porco, C., Strobel, D., Saur, J., Ajello, J., and West, R. 2004. Cassini observations of Io's visible aurorae. *Icarus*, **172**, 127–140.
- Goguen, J. and Blaney, D. L. 2001. Io's 1–2.5 μ m spectrum in eclipse with SpeX at IRTF. *Bull. Amer. Astron. Soc.*, **33**, 24.02.
- Hendrix, A. R., Barth, C. A., and Hord, C. W. 1999. Io's patchy SO₂ atmosphere as measured by the Galileo ultraviolet spectrometer. *J. Geophys. Res.*, **104**, 11817–11826.
- Hinson, D. P., Kliore, A. J., Flasar, F. M., Twickern, J. D., Schinder, P. J., and Herrera, R. G. 1998. Galileo radio occultation measurements of Io's ionosphere and plasma wake. *J. Geophys. Res.*, **103**, 29343–29357.
- Ingersoll, A. P. 1989. Io meteorology: How atmospheric pressure is controlled locally by volcanos and surface frosts. *Icarus*, **81**, 298–313.
- Ingersoll, A. P., Summers, M. E., and Schlipf, S. G. 1985. Supersonic meteorology of Io: Sublimation driven flow of SO₂. *Icarus*, **64**, 375–390.
- Jessup, K. L., Spencer, J. R., Ballester, G. E., Howell, R. R., Roesler, F., Vigel, M., and Yelle, R. 2004a. The atmospheric signature of Io's Prometheus plume and anti-Jovian hemisphere: Evidence for a sublimation atmosphere. *Icarus*, **169**, 197–215.
- Jessup, K. L., Spencer, J., and Yelle, R. 2004b. Variability and Composition of Io's Pele Plume. *Bull. Amer. Astron. Soc.*, **36**, 09.02.
- Jessup, K. L., Ballester, G., Zhu, X., and Combi M. 2005. Io's changing atmosphere: Temporal variability in the SO₂ and SO column densities on Io at eastern and western elongation. *Icarus* (submitted).
- Johnson, R. E. 1989. Plasma heating of an SO₂ atmosphere on Io. *GRL.*, **16**, 1117–1120.
- Johnson, T. V. and Matson, D. L. 1989. Io's tenuous atmosphere. In: S. K. Atreya, J. B. Pollack, and M. S. Matthews (eds), *Origin and Evolution of Planetary and Satellites Atmospheres*. University of Arizona Press, Tucson, AZ, pp. 661–682.
- Johnson, T. V., Matson, D. L., Blaney, D. L., Veeder, G. J., and Davies, A. G. 1995. Stealth plumes on Io. *Geophys. Res. Lett.*, **22**, 3293–3296.
- Kerton, C. R., Fanale, F. P., and Salvail, J. R. 1996. The state of SO₂ on Io's surface. *J. Geophys. Res.*, **101**, 7555–7563.
- Kieffer, S. W. 1982. Dynamics and thermodynamics of volcanic eruption: Implications for the plumes on Io. In: D. Morrison (ed.), *Satellites of Jupiter*. University of Arizona Press, Tucson, AZ, pp. 647–723.
- Kliore, A. J., Cain, D. L., Fjeldbo, G., Siedel, B. L., Sykes, M., and Rasool, S. I. 1974. Preliminary results on the atmospheres of Io and Jupiter from Pioneer 10 S-band occultation experiment. *Science*, **183**, 323–324.
- Kliore, A. J., Fjeldbo, G., Siedel, B. L., Sweetnam, D. N., Sesplaukis, T. T., and Woiceshyn, P. M. 1975. Atmosphere of Io from Pioneer 10 occultation measurements. *Icarus*, **24**, 407–419.

- Kueppers, M. and Schneider, N. M. 2000. Discovery of chlorine in the Io torus. *Geophys. Res. Lett.*, **27**, 513–516.
- Kumar, S. 1980. A model for the atmosphere and ionosphere of Io. *Geophys. Res. Lett.*, **7**, 9–12.
- Kumar, S. 1982. Photochemistry of SO₂ in the atmosphere of Io and implications on atmospheric escape. *J. Geophys. Res.*, **87**, 1677–1693.
- Kumar, S. 1985. The SO₂ atmosphere and ionosphere of Io: Ion chemistry, atmospheric escape, and models corresponding to the Pioneer 10 radio occultation measurements. *Icarus*, **61**, 101–123.
- Kumar, S. and Huntent, D. M. 1982. The atmospheres of Io and other satellites. In: D. Morrison (ed.), *Satellites of Jupiter*. University of Arizona Press, Tucson, AZ, pp. 782–806.
- Kupo, I., Mekler, Y., and Eviatar, A. 1976. Detection of ionized sulfur in the Jovian magnetosphere. *Astrophys. J.*, **205**, L51–L53.
- Lellouch, E. 1996. Urey prize lecture. Io's atmosphere: Not yet understood. *Icarus*, **124**, 1–21.
- Lellouch, E., Belton, M., De Pater, I., Gulkis, S., and Encrenaz, T. 1990. Io's atmosphere from microwave detection of SO₂. *Nature*, **346**, 639–641.
- Lellouch, E., Belton, M., de Pater, I., Paubert, G., Gulkis, S., and Encrenaz, T. 1992. The structure, stability, and global distribution of Io's atmosphere. *Icarus*, **98**, 271–295.
- Lellouch, E., Strobel, D. F., Belton, M. J. S., Summers, M. E., Paubert G., and Moreno, R. 1996. Detection of sulfur monoxide in Io's atmosphere. *Astrophys. J.*, **459**, L107–L110.
- Lellouch, E., Paubert, G., Strobel, D. F., and Belton, M. 2000. Millimeter-wave observations of Io's atmosphere: The IRAM 1999 campaign. *Bull. Amer. Astron. Soc.*, **32**, 3511.
- Lellouch, E., Paubert, G., Moses, J. I., Schneider, N. M., and Strobel, D. F. 2003. Volcanically-emitted sodium chloride as a source for Io's neutral clouds and plasma torus. *Nature*, **421**, 45–47.
- Lopes, R. M. C., Kamp, L. W., Smythe, W. D., Mougini-Mark, P., Kargel, J., Radebaugh, J., Turtle, E. P., Perry, J., Williams, D. A., Carlson, R. W., and Douté, S. 2004. Lava lakes on Io: observations of Io's volcanic activity from Galileo NIMS during the 2001 fly-bys. *Icarus*, **169**, 140–174.
- Lopes-Gautier, R., McEwen, A. S., Smythe, W. B., Geissler, P. E., Kamp, L., Davies, A. G., Spencer, J. R., Keszthelyi, L., Carlson, R., Leader, F. E., *et al.* 1999. Active volcanism on Io: Global distribution and variations in activity. *Icarus*, **140**, 243–264.
- Matson, D. L. and Nash, D. 1983. Io's atmosphere: pressure control by regolith cold trapping and surface venting. *J. Geophys. Res.*, **88**, 4771–4783.
- McEwen, A. S. and Soderblom, L. A. 1983. Two classes of volcanic plumes on Io. *Icarus*, **55**, 191–217.
- McGrath, M. and Johnson, R. E. 1987. Magnetospheric plasma sputtering of Io's atmosphere. *Icarus*, **69**, 519–531.
- McGrath, M. A., Belton, M. J. S., Spencer, J. R., and Sartoretti, P. 2000. Spatially resolved spectroscopy of Io's Pele plume and SO₂ atmosphere. *Icarus*, **146**, 476–493.
- McGrath, M. A., Lellouch, E., Strobel, D. F., Feldman, P. D., and Johnson, R. E. 2004. Satellites atmospheres. In: F. Bagenal, T. Dowling, and W. McKinnon (eds), *Jupiter. The Planet, Satellites, and Magnetosphere*. Cambridge University Press, UK, pp. 457–483.
- Mendillo, M., Wilson, J., Spencer, J., and Stansberry, J. 2004. Io's volcanic control of Jupiter's extended neutral clouds. *Icarus*, **170**, 430–442.
- Morabito, L. A., Synnott, S. P., Kupferman, P. N., and Collins, S. A. 1979. Discovery of currently active extraterrestrial volcanism. *Science*, **204**, 972.
- Moreno, M. A., Schubert, G., Baumgardner, J., Kivelson, M. G., and Paige, D. A. 1991. Io's volcanic and sublimation atmospheres. *Icarus*, **93**, 63–81.

- Morgan, T. H., Potter, A. E., Corliss, J. B., Killen, R.-M., Scherb, F., and Woodward, R. C. 2004. Post-eclipse growth of Io's sodium emissions. *Bull. Amer. Astron. Soc.*, **36**, 1099.
- Moses, J. I., Zolotov, M. Y., and Fegley, B. 2002a. Photochemistry of a volcanically driven atmosphere on Io: Sulfur and oxygen species from a Pele-type eruption. *Icarus*, **156**, 76–106.
- Moses, J. I., Zolotov, M. Y., and Fegley, B. 2002b. Alkali and chlorine photochemistry in a volcanically driven atmosphere on Io. *Icarus*, **156**, 107–135.
- Oliversen, R. J., Scherb, F., Smyth, W. H., Freed, M. E., Woodward Jr., R. C., Marconi, M. L., Retherford, K. D., Lupie, O. L., and Morgenthaler, J. P. 2001. Sunlit Io Atmospheric [OI] 6300 Å emission and the plasma torus. *J. Geophys. Res.*, **106**, 6183–26194.
- Paresce, F., Sartoretti, P., Albrecht, R., Barbieri, C., Blades, J. C., Boksenberg, A., Crane, P., Deharveng, J. M., Disney, M. J., Jakobsen, P., *et al.* 1992. Near-ultraviolet imaging of Jupiter's satellite Io with the Hubble Space Telescope. *Astron. Astrophys.*, **262**, 617–620.
- Pearl, J. C., Hanel, R., Kunde, V., Maguire, W., Fox, K., Gupta, S., Ponnampuruma, C. and Raulin, F. 1979. Identification of gaseous SO₂ and new upper limits for other gases on Io. *Nature*, **288**, 757–758.
- Retherford, K. D. 2002. Io's aurora: HST/STIS observations. PhD thesis, Johns Hopkins University, Baltimore, MD.
- Roesler, F. L., Moos, H. W., Oliversen, R. J., Woodward, R. C., Jr., Retherford, K. D., Scherb, F., McGrath, M. A., Smyth, W. H., Feldman, P. D. and Strobel, D. F. 1999. Far-ultraviolet imaging spectroscopy of Io's atmosphere with HST/STIS. *Science*, **283**, 353–356.
- Sartoretti, P., Belton, M. J. S., and McGrath, M. A. 1996. SO₂ distributions on Io. *Icarus*, **122**, 273–287.
- Sartoretti, P., McGrath, M. A., and Paresce, F. 1994. Disk-resolved imaging of Io with the Hubble Space Telescope. *Icarus*, **108**, 272–284.
- Saur, J. and Strobel, D. F. 2004. Relative contributions of sublimation and volcanoes to Io's atmosphere inferred from its plasma interaction during solar eclipse. *Icarus*, **171**, 411–420.
- Saur, J., Neubauer, F. M., Strobel, D. F., and Summers, M. E. 2000. Io's ultraviolet aurora: Remote sensing of Io's Interaction. *Geophys. Res. Lett.*, **27**, 2893–2896.
- Schaefer, L. and Fegley, B., Jr. 2005. Alkali and halogen chemistry in volcanic gases on Io. *Icarus*, **173**, 454–468.
- Schmitt, B., de Bergh, C., Lellouch, E., Maillard, J.-P., Barbe, A., and Douté, S. 1994. Identification of three absorption bands in the 2- μ m spectrum of Io. *Icarus*, **111**, 79–105.
- Schneider, N. M., Hunten, D. M., Wells, W. K., Schultz, A. B., and Fink, U. 1991. The structure of Io's corona. *Astrophys. J.*, **368**, 298–315.
- Smyth, W. H. and Combi, M. R. 1988. A general model for Io's neutral gas clouds I and II. *Astrophys. J.*, **328**, 397–411.
- Smyth, W. H. and Wong, M. C. 2004. Impact of electron chemistry on the structure and chemistry of Io's atmosphere. *Icarus*, **171**, 171–182.
- Smythe, W. D., Nelson, R. M., and Nash, D. B. 1979. Spectral evidence for SO₂ frost or absorbate on Io's surface. *Nature*, **280**, 766–767.
- Spencer, J. R. and Schneider, N. M. 1996. Io on the eve of the Galileo mission. *Ann. Rev. Astron. Astrophys.*, **24**, 125–190.
- Spencer, J. R., Sartoretti, P., Ballester, G. E., McEwen, A. S., Clarke, J. T. and McGrath, M. A. 1997. Pele plume (Io): Observations with the Hubble Space Telescope. *Geophys. Res. Lett.*, **24**, 2471–2474.
- Spencer, J. R., Lellouch, E., Richter, M. J., López-Valverde, M.-A., Jessup, K. L., Greathouse, T., and Flaud, J.-M. 2005. Mid-infrared detection of large longitudinal asymmetries in Io's SO₂ atmosphere. *Icarus* (in press).

- Spencer, J. R., Jessup, K. L., McGrath, M. A., Ballester, G. E., and Yelle, R. 2000. Discovery of gaseous S₂ in Io's Pele plume. *Science*, **288**, 1208–1210.
- Strobel, D. F. and Wolven, B. C. 2001. The atmosphere of Io: abundances and sources of sulfur dioxide and atomic hydrogen. *Astrophys. Space Sci.*, **277**, 271–287.
- Strobel, D. F., Zhu, X., and Summers, M. E. 1994. On the vertical structure of Io's atmosphere. *Icarus*, **111**, 18–30.
- Summers, M. E. 1985. Theoretical studies of Io's atmosphere. Ph.D. thesis, California Institute of Technology, Pasadena.
- Summers, M. E. and Strobel, D. F. 1996. Photochemistry and vertical transport in Io's atmosphere and ionosphere. *Icarus*, **120**, 290–316.
- Trafton, L. M. 1975. Detection of a potassium cloud near Io. *Nature*, **258**, 690–692.
- Trafton, L. M., Matson, D. L., and Stansberry, J. A. 1995. Surface/atmosphere interaction and volatile transport (Triton, Pluto and Io). Submitted to *Solar System Ices*, eds. B. Schmitt, C. de Bergh, and M. Festou, Kluwer Academic, Dordrecht, The Netherlands.
- Trafton, L. M., Caldwell, J. J., Barnet, C., and Cunningham, C. C. 1996. The gaseous sulfur dioxide abundance over Io's leading and trailing hemispheres: HST spectra of Io's C¹B₂–X¹A₁ band of SO₂ near 2,100 Å. *Astrophys. J.*, **456**, 384–392.
- Wilson, J. K. and Schneider, N. M. 1994. Io's fast sodium: Implications for molecular and atomic escape. *Icarus*, **111**, 31–44.
- Wolven, B. C., Moos, H. W., Retherford, K. D., and Feldman, P. D. 2001. Emission Profiles of neutral oxygen and sulfur in Io's exospheric corona. *J. Geophys. Res.*, **106**, 26155–16182.
- Wong, M. C. and Johnson, R. E. 1995. The effect of plasma heating on sublimation-driven flow in Io's atmosphere. *Icarus*, **155**, 109–118.
- Wong, M. C. and Johnson, R. E. 1996. A three-dimensional azimuthally symmetric model atmosphere for Io. 1: Photochemistry and the accumulation of a nightside atmosphere. *J. Geophys. Res.*, **101**, 23243–23254.
- Wong, M. C. and Smyth, W. H. 2000. Model calculations for Io's atmosphere at eastern and western elongations. *Icarus*, **146**, 60–74.
- Wu, R. C. Y., Yang, B. W., Chen, F. Z., Judge, J., Caldwell, J., and Trafton, L. M. 2000. Measurements of high-, room-, and low-temperature photoabsorption cross sections of SO₂ in the 2080- to 2950-Å region, with applications to Io. *Icarus*, **145**, 289–296.
- Zhang, J., Goldstein, D. B., Varghese, P. L., Gimelshein, N. E., Gimelshein, S. F., and Levin, D. A. 2003. Simulation of gas dynamics and radiation in volcanic plumes of Io. *Icarus*, **163**, 182–187.
- Zhang, J., Goldstein, D. B., Varghese, P. L., Trafton, L., Moore, C., and Miki, K. 2004. Numerical modeling of ionian volcanic plumes with entrained particulates. *Icarus*, **172**, 479–502.
- Zolotov, M. Yu. and Fegley, B. Jr. 1998a. Volcanic production of sulfur monoxide (SO) on Io. *Icarus*, **132**, 431–434.
- Zolotov, M. Yu. and Fegley, B. Jr. 1998b. Volcanic origin of disulfur monoxide (S₂O) on Io. *Icarus*, **133**, 293–297.
- Zolotov, M. Yu. and Fegley, B. Jr. 1999. Oxidation state of volcanic gases and the interior of Io. *Icarus*, **141**, 40–52.
- Zolotov, M. Yu. and Fegley, B. Jr. 2000. Eruption conditions of Pele volcano on Io inferred from chemistry of its volcanic plume. *Geophys. Res. Lett.*, **27**, 2789–2792.

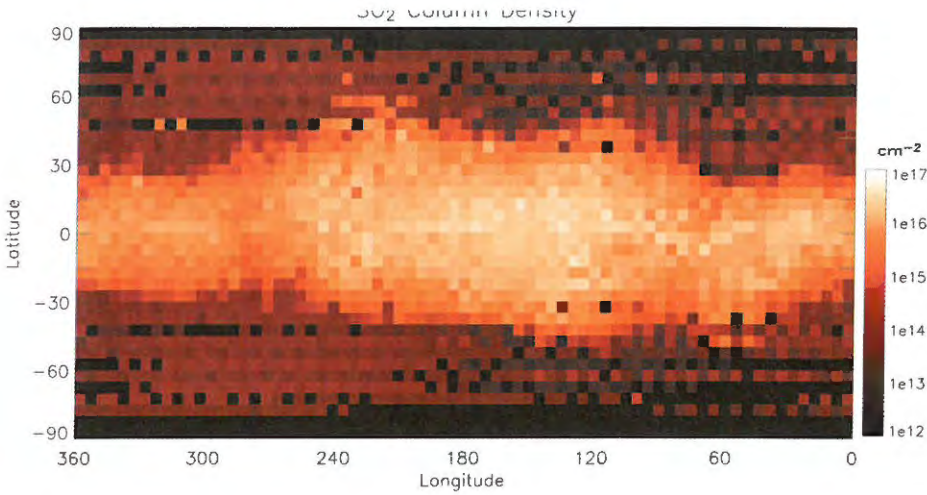


Figure 10.4. 2-D SO₂ gas distribution, as inferred from Ly α images (from Feaga *et al.*, 2004a).

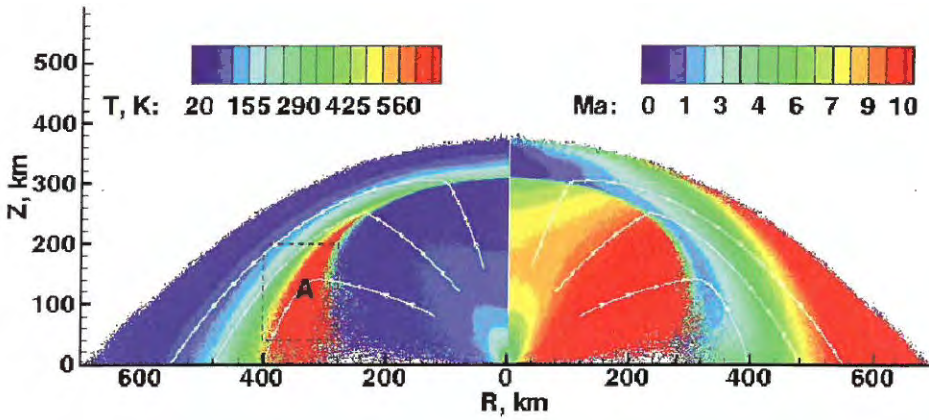


Figure 10.7. Model of an isolated Pele-type volcanic plume. Contours of the temperature and Mach number are shown (from Zhang *et al.*, 2003).